HHS Public Access

Author manuscript

J Am Chem Soc. Author manuscript; available in PMC 2022 January 17.

Published in final edited form as:

J Am Chem Soc. 2021 July 14; 143(27): 10462–10476. doi:10.1021/jacs.1c05470.

Amphiphilic Distyrylbenzene Derivatives as Potential Therapeutic and Imaging Agents for Soluble and Insoluble Amyloid β Aggregates in Alzheimer's Disease

Liang Sun,
Department of Chemistry, Beckman Institute for Advanced Science and Technology, The Neuroscience Program, University of Illinois at Urbana–Champaign, Urbana, Illinois 61801, United States

Hong-Jun Cho,
Department of Chemistry, Beckman Institute for Advanced Science and Technology, The Neuroscience Program, University of Illinois at Urbana–Champaign, Urbana, Illinois 61801, United States

Soumyo Sen,
NIH Center for Macromolecular Modeling and Bioinformatics, Beckman Institute for Advanced Science and Technology, Center for Biophysics and Quantitative Biology and Department of Biochemistry, University of Illinois at Urbana–Champaign, Urbana, Illinois 61801, United States

Andres S. Arango,
NIH Center for Macromolecular Modeling and Bioinformatics, Beckman Institute for Advanced Science and Technology, Center for Biophysics and Quantitative Biology and Department of Biochemistry, University of Illinois at Urbana–Champaign, Urbana, Illinois 61801, United States

Truc T. Huynh,
Department of Radiation Oncology, Washington University School of Medicine, St. Louis, Missouri 63108, United States; Department of Chemistry, Washington University, St. Louis, Missouri 63130, United States

Yiran Huang,
Department of Chemistry, Beckman Institute for Advanced Science and Technology, The Neuroscience Program, University of Illinois at Urbana–Champaign, Urbana, Illinois 61801, United States

Nilantha Bandara,
Department of Radiation Oncology, Washington University School of Medicine, St. Louis, Missouri 63108, United States

Corresponding Author: Liviu M. Mirica – mirica@illinois.edu.

Supporting Information

The Supporting Information is available free of charge at https://pubs.acs.org/doi/10.1021/jacs.1c05470.

General methods, synthetic details, fluorescence imaging studies, and molecular docking studies, animal studies, and radiochemistry studies (PDF)

Complete contact information is available at: https://pubs.acs.org/10.1021/jacs.1c05470

The authors declare no competing financial interest.

Buck E. Rogers,
Department of Radiation Oncology, Washington University School of Medicine, St. Louis, Missouri 63108, United States

Emad Tajkhorshid,
NIH Center for Macromolecular Modeling and Bioinformatics, Beckman Institute for Advanced Science and Technology, Center for Biophysics and Quantitative Biology and Department of Biochemistry, University of Illinois at Urbana–Champaign, Urbana, Illinois 61801, United States

Liviu M. Mirica
Department of Chemistry, Beckman Institute for Advanced Science and Technology, The Neuroscience Program, University of Illinois at Urbana–Champaign, Urbana, Illinois 61801, United States; Hope Center for Neurological Disorders, Washington University School of Medicine, St. Louis, Missouri 63110, United States

Abstract

Alzheimer's Disease (AD) is the most common neurodegenerative disease, and efficient therapeutic and early diagnostic agents for AD are still lacking. Herein, we report the development of a novel amphiphilic compound, LS-4, generated by linking a hydrophobic amyloid-binding distyrylbenzene fragment with a hydrophilic triazamacrocycle, which dramatically increases the binding affinity toward various amyloid β (Aβ) peptide aggregates, especially for soluble Aβ oligomers. Moreover, upon the administration of LS-4 to 5xFAD mice, fluorescence imaging of LS-4-treated brain sections reveals that LS-4 can penetrate the blood-brain barrier and bind to the Aβ oligomers *in vivo.* In addition, the treatment of 5xFAD mice with LS-4 reduces the amount of both amyloid plaques and associated phosphorylated tau aggregates vs the vehicle-treated 5xFAD mice, while microglia activation is also reduced. Molecular dynamics simulations corroborate the observation that introducing a hydrophilic moiety into the molecular structure of LS-4 can enhance the electrostatic interactions with the polar residues of the Aβ species. Finally, exploiting the Cu^{2+}-chelating property of the triazamacrocycle, we performed a series of imaging and biodistribution studies that show the ^{64}Cu-LS-4 complex binds to the amyloid plaques and can accumulate to a significantly larger extent in the 5xFAD mouse brains vs the wild-type controls. Overall, these results illustrate that the novel strategy, to employ an amphiphilic molecule containing a hydrophilic moiety attached to a hydrophobic amyloid-binding fragment, can increase the binding affinity for both soluble and insoluble Aβ aggregates and can thus be used to detect and regulate various Aβ species in AD.

Graphical Abstract

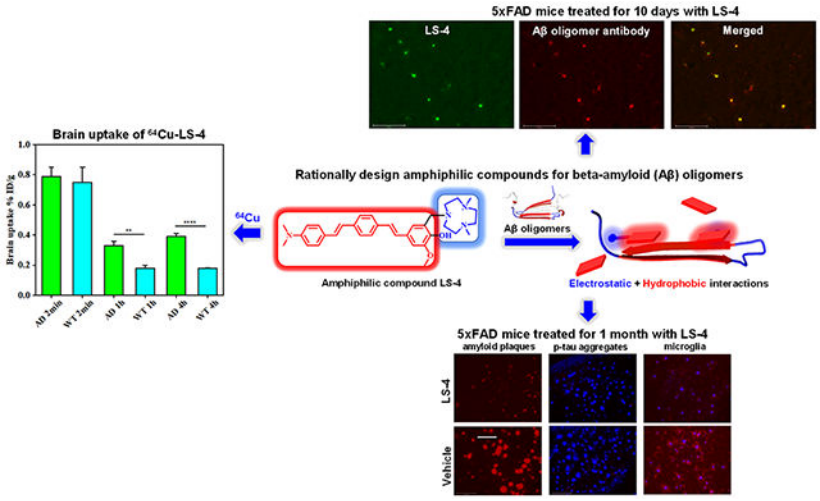

INTRODUCTION

Alzheimer's Disease (AD), the most prevalent neurodegenerative disease, currently affects almost 6 million people in the US and 44 million worldwide.[1] Unfortunately, AD is still an irremediable disorder with a complex pathology, which poses tremendous challenges for the development of improved therapeutic and diagnostic tools.[2,3] The formation of extracellular amyloid plaques containing the amyloid β (Aβ) peptide is one of the pathological hallmarks of the brains of AD patients,[4,5] and this led to the amyloid-cascade hypothesis that states the amyloid plaque formation initiates cellular events that lead to neurodegeneration.[6,7] However, recent studies indicate that the deposition of amyloid plaques does not correlate with the progression of AD, instead soluble Aβ oligomers are believed to play a significant role, as they lead to synaptic dysfunction and memory loss in AD patients and AD animal models.[8–10] Though the exact pathological mechanism of soluble Aβ oligomers is still not clear, more clinical trials have shown that the targeting of neurotoxic soluble Aβ oligomers instead of insoluble Aβ fibrils is a more effective strategy to slow down the progression of AD.[11,12] Consequently, we think it is very important to develop improved therapeutic and diagnostic tools to detect and characterize these soluble Aβ species.

Fluorescence probes for amyloid fibrils have been developed and widely used during the past two decades.[13–16] These probes can specifically bind to the amyloid plaques in AD patients and AD models. Furthermore, several positron emission tomography (PET) compounds have been developed and approved by the FDA and can be used to visualize amyloid plaques in AD patients.[17–19] The main strategy to develop such imaging agents is to employ hydrophobic π-conjugated aromatic systems that interact with the hydrophobic residues in the β-sheet cores of the amyloid fibrils through hydrophobic–hydrophobic interactions. However, most of the probes can only recognize the insoluble, fibrillar Aβ species and have a poor ability to detect the most neurotoxic soluble Aβ oligomers.

Recently, novel fluorescent dyes that can bind soluble Aβ oligomers have been reported.[20–27] However, the discovery of these molecules is normally achieved via high throughput screening or limited structure–activity relationship studies, and there are

no general guidelines to rationally design a soluble Aβ oligomer probe. In addition, numerous studies have shown that multifunctional compounds (MFCs) that contain an Aβ fibril-binding fragment and additional moieties that target other AD pathologies (e.g., as metal ion dishomeostasis,[28–33] reactive oxygen species (ROS) formation,[34–36] neuroinflammation,[37,38] and acetylcholinesterase inhibition[39,40]) could be potential lead compounds for AD therapeutics development.[41–45] However, to the best of our knowledge, to date no MFCs have been developed that exhibit appreciable affinity for the soluble Aβ oligomers and target also other AD pathologies.

Herein, we report the development of a novel amphiphilic compound, LS-4, generated by linking a hydrophobic amyloid fibril-binding fragment with a hydrophilic azamacrocycle that can dramatically increase the binding affinity toward various amyloid β (Aβ) peptide aggregates (Figure 1). The developed compound exhibits uncommon fluorescence turn-on and high binding affinity for Aβ aggregates, especially for soluble Aβ oligomers. By comparison, the compound Pre-LS-4, which contains only the hydrophobic conjugated aromatic fragment without the hydrophilic azamacrocycle moiety, exhibits significantly reduced binding affinity for the Aβ species. LS-4 also exhibits antioxidant properties and can arrest the Cu^{2+}-ascorbate redox cycling that can lead to ROS formation. Moreover, upon the administration of LS-4 to 5xFAD mice, fluorescence imaging of the LS-4-treated brain sections reveals that LS-4 can readily penetrate the blood-brain-barrier (BBB) and bind to the Aβ oligomers *in vivo*, as confirmed by immunostaining with an Aβ oligomer-specific antibody. In addition, the treatment of 5xFAD mice with LS-4 significantly reduces the amount of both amyloid plaques and associated phosphorylated tau (p-tau) aggregates vs the vehicle-treated 5xFAD mice, while microglia activation is also reduced. Furthermore, molecular dynamics (MD) simulations corroborate the observation that introducing a hydrophilic moiety into the molecular structure can significantly enhance the electrostatic interactions with the polar residues of the Aβ peptide species. Finally, taking advantage of the strong Cu-chelating property of the azamacrocycle, we performed a series of positron emission tomography (PET) imaging and biodistribution studies that show the ^{64}Cu-LS-4 complex binds to the amyloid plaques and can accumulate to a significantly larger extent in the 5xFAD mouse brains vs the WT controls. Overall, these *in vitro* and *in vivo* studies illustrate that the novel strategy to employ an amphiphilic molecule containing a hydrophilic fragment attached to a hydrophobic amyloid fibril-binding fragment can increase the binding affinity of these compounds for the soluble Aβ oligomers and can thus be used to detect and regulate the soluble Aβ species in AD.

RESULTS AND DISCUSSION

Synthesis of LS-4 and Pre-LS-4.

Recent reports focusing on the soluble Aβ oligomer structures have shown that the surfactant-stabilized soluble Aβ aggregates possess an amphiphilic property, including hydrophobic cores and water-soluble hydrophilic regions.[46–48] This type of structure is proposed to promote the interaction of the soluble Aβ oligomers with the lipid membranes and generate pores and channel-like structures that may also disrupt the neuron cell membrane integrity.[49–53] Thus, attaching hydrophilic moieties to hydrophobic Aβ fibril-

binding fragments can be an effective strategy to design small molecules to probe the soluble Aβ oligomers, since such a amphiphilic molecule can interact with the both the hydrophobic regions as well as the hydrophilic residues of the soluble Aβ oligomers. Based on this strategy, the amphiphilic compound LS-4 contains a hydrophilic azamacrocycle, 2,4-dimethyl-1,4,7-triazacyclononane (Me_2HTACN), and a hydrophobic distyrylbenzene derivative known to exhibit high binding affinity for the Aβ species (Figure 1).[54,55] The novel asymmetric distyryl stilbene derivative contains fragments resembling the FDA-approved PET imaging agent [^{18}F]florbetaben, the symmetric distyrylbenzene structure of compound DF-9 and the related methoxy-X04–which have been widely used in detecting amyloid plaques,[18,56,57] as well as the 2-methoxy-phenol fragment reminiscent of o-vanillin that was shown to inhibit the formation of Aβ oligomers and also exhibit antioxidant properties.[58] Notably, a similar type of unsymmetric distyrylbenzene structure has been used for membrane potential sensor development,[59] yet it has never been utilized for binding to or detecting Aβ species related to AD. The synthesis of LS-4 employs a Heck reaction to generate the Pre-LS-4 compound first,[60] followed by the Mannich reaction with paraformaldehyde and the Me_2HTACN azamacrocycle fragment to yield LS-4 (Scheme 1).

Fluorescence Turn-on Effect of LS-4 and Pre-LS-4 with Aβ Species.

To probe whether the introduction of the hydrophilic azamacrocycle moiety into the Aβ fibril-binding fragment can increase the interaction toward various Aβ species (Figure 1), a fluorescence turn-on assay was performed to evaluate whether LS-4 can interact with both the soluble Aβ oligomers and insoluble Aβ aggregates. Interestingly, LS-4 shows a remarkable fluorescence turn-on effect (~20 fold) when added to a solution of Aβ_{42} fibrils (Figure 2a). We have also prepared Aβ_{42} oligomers according to the procedure reported by Klein[61] and confirmed their morphology by transmission electron microscope (TEM, Figure S2). Notably, in the presence of Aβ_{42} oligomers, LS-4 shows a more significant 50-fold fluorescence turn-on effect than in the presence of Aβ_{42} fibrils. Furthermore, when comparing with the emission spectra of LS-4 with fibrils and Aβ oligomers, the maximum emission wavelength of LS-4 shows a blue shift from 500 to 470 nm, respectively, probably due to the compound binding to a more hydrophobic region of the Aβ oligomers, and thus suggesting LS-4 may be useful as a structure-specific or polymorph-specific dye to detect both Aβ oligomers and fibrils. By comparison, the Pre-LS-4 compound, which does not contain the hydrophilic triazamacrocycle group, only exhibits a small turn-on effect in the presence of either the Aβ_{42} oligomers or fibrils (Figure 2b). This result strongly suggests that the hydrophilic azamacrocycle present in LS-4 enhances the fluorescence turn-on effect in the presence of Aβ species, especially the soluble Aβ_{42} oligomers.

The triazamacrocycle moiety is known to act as a strong metal-chelating ligand, including binding to Cu^{2+} ions.[28–33] On the basis of the predicted pK_a values for LS-4 (see the Supporting Information) and the previously reported triazamacrocycle-phenol derivatives,[28–33] LS-4 is expected to be monoprotonated at pH 7.4, with the N atoms of the triazamacrocyle interacting with the proton. Moreover, it is expected that upon chelating to Cu^{2+}, LS-4 will undergo deprotonation of the phenol group and thus the Cu^{2+}-LS-4 complex will be monocationic and should exhibit similar amyloid binding properties as LS-4. As a result, we have employed the Cu-LS-4 complex to probe its fluorescence properties when

interacting with the Aβ_{42} oligomers and fibrils. Interestingly, when the Cu-LS-4 complex was added to the Aβ_{42} oligomers or fibrils, it exhibits similar fluorescence turn-on effects as LS-4 (Figure S3). Overall, the fluorescence turn-on results clearly indicate that improving the hydrophilicity of the compound can significantly enhance the binding affinity toward Aβ oligomers and fibrils.

Binding Affinity LS-4 and Pre-LS-4 to Aβ_{42} Oligomers and Fibrils.

To explore further the binding affinity toward Aβ_{42} species, we used different Aβ_{42} species and direct-binding fluorescent assays to measure the K_d values for the developed compounds. LS-4 displays nanomolar affinity for the Aβ_{42} oligomers (K_d = 50 ± 9 nM) and fibrils (K_d = 58 ± 15 nM), indicating that the developed compounds bind tightly not only to the amyloid fibrils but also to the soluble Aβ_{42} oligomers (Figure 3). However, in the absence of the hydrophilic azamacrocycle fragment, the binding affinity of Pre-LS-4 toward the amyloid species dramatically decreased to 9–10 μM (Figure S4), strongly suggesting that the hydrophilic moiety plays a significant role in binding to the Aβ_{42} species.

Monitoring of Kinetics of Aβ_{42} Aggregation.

Following the fluorescence turn-on effect studies, the Aβ_{42} oligomersensing properties of LS-4 were probed during Aβ_{42} aggregation. The on-pathway aggregation conditions were employed for the growth of Aβ_{42} fibrils,[61] and the whole aggregation process was monitored by thioflavin T (ThT) fluorescence. In addition, at each selected time point an aliquot of LS-4 was added to the Aβ_{42} solution and its fluorescence intensity was measured. Interestingly, the LS-4 emission intensity increased at the beginning and reached the maximum after ~2 h of incubation and then decreased dramatically during the following 48 h of incubation, while the ThT emission intensity increased steadily (Figure 4). These observed changes in the fluorescence intensity suggests that LS-4 detects the on-pathway Aβ_{42} oligomers, with its fluorescence signal increasing as the monomeric Aβ_{42} aggregates into oligomers, and then decreases as Aβ_{42} fibrils are formed in solution. By comparison, when similar kinetics studies were performed with Pre-LS-4, its emission intensity decreased significantly in the first 1 h and then reached a plateau during the extended incubation time, suggesting that Pre-LS-4 does not follow the same behavior to detect Aβ_{42} oligomers as LS-4, while also showing a limited Aβ fibril-binding turn-on fluorescence. This result further highlights the importance of the hydrophilic azamacrocycle fragment for binding to the soluble Aβ_{42} oligomers (Figure S5a). Moreover, the Aβ aggregation process was also monitored with the Cu-LS-4 complex, which interestingly shows a similar trend as LS-4 when tracking the Aβ_{42} aggregation process (Figure S5b). The fluorescence intensity increases in line with the formation of the Aβ_{42} oligomers, and then decreases as the Aβ_{42} fibrils are formed in solution, indicating the Cu^{2+}-LS-4 complex also has the capacity to detect the soluble Aβ_{42} oligomers, and this property could be used for ^{64}Cu PET imaging applications (see below).

Fluorescence Staining of 5xFAD Mouse Brain Sections.

To investigate further the selective binding of LS-4 and Pre-LS-4 to the various Aβ species, these compounds were used in *ex vivo* fluorescence imaging studies. The brain sections of 7-month old 5xFAD transgenic mice, which rapidly develop severe amyloid

pathology,[62] were stained with LS-4 and then sequentially stained with either Congo Red (a well-known fluorescent dye)[63] or immunostained with the HJ3.4 antibody, which can bind to a wide range of Aβ species,[64] or with an Aβ oligomer-specific monoclonal antibody (OMAB), which specifically binds to Aβ oligomers.[21,22,65,66] A strong fluorescence signal was detected upon staining of the 5xFAD mouse brain sections with LS-4 (Figure 5, left panels), with an excellent colocalization with the immunofluorescence of OMAB (Pearson's correlation coefficient of 0.89). For the brain sections immunostained with HJ3.4, the colocalization of the LS-4 signal was also high (Pearson's correlation coefficient 0.78), since the HJ3.4 antibody can bind to a wide range of Aβ species. These results indicate that LS-4 could probe both the Aβ oligomers and fibrils in AD brain sections. By comparison, when the brain sections were treated with Pre-LS-4, the fluorescence images show the colocalization between the compound and HJ3.4 antibody is much lower than that for LS-4 (Figure S6). This result also suggests that the TACN azamacrocycle is essential for Aβ binding, which is consistent with the *in vitro* fluorescence turn-on studies. The brain sections from 5xFAD mice of different ages considered as early (3-month old), middle (7-month old), and late stage (11-month old) were used to perform the staining studies. These images show that LS-4 can efficiently and clearly label amyloid plaques for all three different ages, while for Pre-LS-4 the fluorescence intensity is significantly lower under the same conditions as LS-4 (Figure S7). To explore further the affinity of the Cu^{2+}-LS-4 complex toward the Aβ aggregates, the 5xFAD mouse brain sections were stained with the Cu^{2+}-LS-4 complex followed by either Congo Red staining, or HJ3.4 antibody staining, or OMAB antibody staining. The fluorescence images show that the Cu^{2+}-LS-4 complex has fairly good colocalization with Congo red, HJ3.4, and OMAB, indicating that Cu^{2+}-LS-4 exhibits the ability to selectively bind Aβ species *ex vivo*, similarly to LS-4 (Figure S8). This lends further support to the possibility of using ^{64}Cu-LS-4 as a ^{64}Cu PET imaging agent for amyloid plaques in AD (see below).

Trolox Equivalent Antioxidant Capacity Assays.

Trolox-Equivalent Antioxidant Capacity (TEAC) assays were employed to evaluate the antioxidant ability of the Pre-LS-4 and LS-4 compounds, both of which contain a 2-methoxyphenol group. The TEAC assays have been widely used for measuring the antioxidant activity of foods by monitoring via UV–vis the disappearance of the $ABTS^{+\bullet}$ radical cation.[67] Trolox, a water-soluble analogue of vitamin E, has strong antioxidant properties and was used as a standard.[68] In addition, Pre-LS-4 and LS-4 were also compared with glutathione, which has an appreciable antioxidant ability and plays a fundamental role in detoxification of ROS.[69] Interestingly, both Pre-LS-4 and LS-4 show very good antioxidant capacity compared to Trolox (Figure 6), indicating that both compounds can quench the radical species efficiently and protect the cells from oxidative stress, likely due to the electron-rich 2-methoxyphenol fragment present in both compounds.

Cu^{2+}-Induced Ascorbate Consumption Assays.

It is known that the Cu^{2+}-Aβ_{42} species can promote the formation of ROS that have deleterious effects in AD.[70] Herein, we employed an ascorbate consumption assay to evaluate the ability of LS-4 to suppress the Cu^{2+}-ascorbate redox cycling. In the absence of LS-4, the consumption of ascorbate in the presence of Cu^{2+} is rapid (Figure 7a, black).

However, if Cu^{2+} is premixed with 2 eq of LS-4, the ascorbate consumption is almost completely abolished (Figure 7a, red), indicating that LS-4 can bind tightly to Cu^{2+} and mitigate the redox cycling. Furthermore, with the addition of LS-4 into the Cu^{2+}-ascorbate solution, the consumption of ascorbate can be arrested immediately and significantly (Figure 7a, blue), showing that the LS-4 can efficiently regulate the redox process. We also performed the ascorbate consumption assay in the presence of $A\beta_{42}$, mimicking conditions that are more relevant to those in AD. In comparison with that in the Cu^{2+}-$A\beta_{42}$ species, addition of 2 eq LS-4 leads to a significant inhibition of ascorbate consumption (Figure 7b), suggesting that LS-4 can bind strongly to Cu^{2+} and silence the Cu^{2+}-ascorbate redox cycling in the presence of $A\beta_{42}$ species.

These results show that LS-4 can efficiently chelate Cu^{2+} to prevent its reduction by ascorbate, even in the presence of the $A\beta$ species, and thus inhibit the formation of ROS upon redox cycling. By comparison, the addition of Pre-LS-4 does not affect the rate of ascorbate consumption via Cu^{2+}-ascorbate redox cycling (Figure S9), as expected since Pre-LS-4 is missing the metal-chelating triazamacrocycle fragment.

Attenuation of Copper-Induced $A\beta_{42}$ Cytotoxicity by LS-4.

Since the Cu^{2+}-$A\beta_{42}$ species were shown to be neurotoxic,[71] it is important to develop novel metal-chelating compounds that can control the Cu^{2+}-induced $A\beta_{42}$ cytotoxicity. In this respect, we investigated the effect of LS-4 to alleviate the neurotoxicity of Cu-$A\beta_{42}$ species in N2a cells by using the Alamar blue cell viability assay.[72] Interestingly, in the presence of both $A\beta_{42}$ and Cu^{2+}, LS-4 can rescue the viability of N2a cells and significantly alleviate the neurotoxicity of Cu^{2+}- $A\beta_{42}$ species (Figure S11). Overall, the above antioxidant, redox cycling, and cytotoxicity studies suggest that LS-4 could be a useful modulator of the oxidative stress and ROS formation promoted by the $A\beta_{42}$ species in the context of AD.

Treatment of 5xFAD transgenic mice.

The BBB permeability of promising compounds is highly crucial for any *in vivo* applications. In order for the compounds to penetrate the BBB, their lipophilicity (i.e., logP or logD values) should be within the 0.9–2.5 range.[73] Since the structure of LS-4 contains a hydrophilic azamacrocycle fragment, it is important to confirm that LS-4 still possesses enough lipophilicity to cross the BBB. The lipophilicity of the compounds was determined by measuring the octanol/PBS (pH 7.4) partition coefficients logD. For Pre-LS-4, a higher logD value of 1.22 ± 0.04 was found, while LS-4 exhibits a logD value of 0.98 ± 0.13, suggesting that LS-4 should still be able to cross the BBB. Encouraged by this result, LS-4 was administered daily (1 mg/kg of body weight) to 7-month old 5xFAD mice for 10 days via intraperitoneal injection. The brain sections of the LS-4-treated mice displayed a remarkably strong fluorescence for the accumulated LS-4 binding to the $A\beta$ species (Figure 8, left panel). Fluorescence and immunohistochemical staining was employed to confirm the $A\beta$-binding specificity of LS-4. First, the LS4-treated 5xFAD brain sections were stained with Congo Red, which is known to stain the mature amyloid fibrils,[63] and the colocalization images show LS-4 can label a wider range of $A\beta$ species than Congo Red (Figure 8, top panel). Then, the brain sections were immunostained with the pan-$A\beta$ antibody HJ3.4, which can recognize a wide range of $A\beta$ species,[64] and the fluorescence

images show that the HJ3.4-stained regions are slightly larger than the LS-4-stained regions, although an appreciable colocalization was observed (Figure 8, middle panel). Finally, brain sections were treated with OMAB that can stain the Aβ oligomers specifically,[65] and these images demonstrated that LS-4 exhibits excellent colocalization with OMAB, supporting that LS-4 has the ability to bind the soluble Aβ oligomers (Figure 8, bottom panel). Consequently, all these data strongly support that LS-4 can efficiently penetrate the BBB and bind to both Aβ oligomers and fibrils, which is consistent with the *ex vivo* studies.

In Vivo Regulation of Aβ Species.

To evaluate the *in vivo* therapeutic efficacy of LS-4, we have administered the LS-4 compound daily (1 mg/kg of body weight) to 5xFAD mice via intraperitoneal injection for 30 days. Since the amyloid plaques began to deposit in the deep cortex and subiculum of 5xFAD mice starting as early as 2 months of age,[62] 3-month old 5xFAD mice were selected that contain multiple forms of Aβ species, including Aβ monomers, soluble Aβ oligomers, intraneuronal Aβ aggregates, and amyloid plaques.[74] Other 5xFAD mice were treated with the vehicle (1% DMSO in PBS) daily as the control group. After the 30-day treatment, the brains were harvested and 50 μm thick brain sections were obtained. For the quantitative analysis of all amyloid aggregates, immunostaining with the CF594-HJ3.4 antibody was performed for the treated 5xFAD mice brain sections. We have quantified the amyloid plaques in the brain sections by analyzing the area of the antibody-stained plaques of 8 brain sections per mouse that were sliced from uniformly distributed locations between the frontal lobe and the occipital lobe (Figure 9a). For each brain section, 5 regions throughout the cortex area were randomly selected and the areas of antibody-stained amyloid plaques were quantified. The fluorescence images show that the areas of HJ3.4-labeled amyloid aggregates were significantly reduced by 60% in the LS-4-treated brain sections vs the vehicle-treated 5xFAD mice brain sections (Figure 9b). To confirm the ability of LS-4 to modulate the Aβ aggregation process *in vivo*, the total amount of cerebral Aβ_{40} and Aβ_{42} peptides were quantified by using and Aβ enzyme-linked immunosorbent assay (ELISA). Importantly, the amount of PBS-soluble and guanidine-soluble Aβ_{42} peptide was reduced significantly by 66% and 72%, upon treatment with LS-4 vs vehicle, respectively (Figure 9c). In addition, the levels of guanidine-soluble Aβ_{40} peptide also drastically decreased by 76% (Figure S12). Overall, these results indicate that LS-4 is able to significantly delay and mitigate the aggregation of Aβ species in 5xFAD mice via strong interactions with both Aβ oligomers and fibrils.

Attenuation of Aβ-Induced p-Tau Aggregation and Neuroinflammation in 5xFAD Mice.

Recently, several clinical trials focusing on Aβ-targeting therapeutics have failed,[75,76] and the amyloid cascade hypothesis is being re-evaluated and new therapeutics are now focusing on additional pathologies such as p-tau aggregation and neuroinflammation. Therefore, it has been proposed that therapeutic agents targeting also the tau pathology and neuroinflammation could be more effective than Aβ-targeting-only therapeutics, since tau hyperphosphorylation and p-tau aggregates are more closely correlated to the cognitive and clinical symptoms of AD than the amyloid plaques formation. However, the amyloid plaques have been shown to facilitate the initial p-tau aggregation surrounding the amyloid plaques and the spread of formation of the intracellular neurofibrillary tangles (NFT).[77,78] Therefore,

we investigated the effect of LS-4 on the aggregation of p-tau protein and the activation of microglia as a neuroinflammatory response. Although the 5xFAD mouse model does not exhibit an obvious tau pathology, a substantial amount of extracellular p-tau aggregates are still observed in the cortex and hippocampus regions of the 5xFAD mice.[79] Therefore, a fluorescently labeled AT8 antibody, which can specifically recognize the p-tau aggregates, was employed to immunostain the p-tau aggregates surrounding the amyloid plaques and allow for their quantification (Figure 10a). We found that the amount of p-tau aggregates surrounding the amyloid plaques were significantly decreased by 47% in the LS-4-treated vs vehicle-treated 5xFAD mice (Figures 10b, S13). This result is exciting, since recent amyloid-targeting immunotherapies showed the Aβ specific antibodies efficiently reduce the Aβ deposition, yet they have no effect on p-tau aggregation *in vivo*.[80–83] Although the role of Aβ species in the initial p-tau aggregation and the formation of intracellular NFT is still not clear, these results suggest that LS-4 decreases the amount of p-tau aggregates surrounding the amyloid plaques. Since it was shown that soluble Aβ oligomers and Aβ fibrils can bind to and activate the microglial cells via cell-surface receptors to initiate a neuroinflammatory response and inducing neuron injury in AD, it is important to evaluate the level of activated microglia cells in AD mice.[84,85] Therefore, the CF594-labeled ionized calcium-binding adapter molecule 1 (Iba1) antibody[86] was employed to detect via immunofluorescence staining the Iba1 protein, which is specifically expressed in microglia cells. Strikingly, the amount of Iba1 was significantly reduced near the amyloid plaques upon treatment with LS-4, with the fluorescence intensity of Iba1 antibody being reduced by 52% vs the vehicle-treated 5xFAD mice (Figures 10c, S14), indicating LS-4 could suppress the activation of microglia cells to alleviate the neuroinflammation in 5xFAD mice. These results further support that LS-4 can regulate the Aβ aggregation process and alleviate the Aβ-induced neurotoxicity, leading to the attenuation of neuroinflammation mediated by microglia activation near the amyloid plaques.

Docking studies and MD simulations.

To gain molecular insight into the nature of the interactions of LS-4 with the Aβ aggregates, molecular docking and MD simulations[87,88] were performed to characterize the binding of LS-4 to both soluble Aβ oligomers and Aβ fibrils. First, LS-4 and Pre-LS-4 were docked onto the NMR-resolved Aβ fibril structure (PDB ID: 2LMN)[89] as well as onto the recently reported NMR/MD structure of the lipid membrane-bound Aβ_{42} octamer (PDB ID: 6RHY).[47] Interestingly, analysis of large ensembles of tens of thousands of poses of the two compounds docked onto the two protein structures show that LS-4 mainly occupies the two ends of the fibril in a partially inserted configuration (Figures 11a, S15a), whereas Pre-LS-4 can be evenly distributed in the entire fibril cavity (Figures 11b, S15b). This docking result also lends support that compound LS-4 can efficiently restrict the fibril formation *in vivo* probably due to the preferential binding to the fibril ends of LS-4 to mitigate the Aβ elongation process. In contrast to the Aβ fibril, there is almost no difference in the occupancy map of LS-4 and Pre-LS-4 for the Aβ oligomer (Figure S16). MD simulations were performed for the most energetically favorable poses, followed by interaction energy calculations of the two compounds and the two protein structures. Although the van der Waals interaction energies between Pre-LS-4 and LS-4 with the Aβ fibril are very similar, the presence of the TACN azamacrocycle in LS-4 increases

the electrostatic coupling originating from the interactions between the amine groups and ASP23 of the Aβ peptide (Figure 11c), while multiple nonpolar amino acids such as PHE19, ALA21, ALA30 and ILE32 are surrounding the phenyl-vinylene fragments for both LS-4 and Pre-LS-4. Moreover, similar to the LS-4-Aβ fibril interactions, LS-4 provides stronger electrostatic interactions than Pre-LS-4 with the Aβ oligomer embedded into the lipid bilayer (Figure S17). In this case, a membrane curvature occurs as a result of hydrophilic side chains attracting water and lipid head groups, forming water pores and causing nearby lipids to curve along the water pores. Although the planar portion of LS-4 and Pre-LS-4 both intercalate in between the octamer leaflets, interaction energy analysis finds that the TACN azamacrocycle in LS-4 experiences electrostatic stabilization via the curved, neighboring lipid head groups (Figure S17a). This effect allows LS-4 to make favorable electrostatic interactions with the solvent and the lipid head groups, which is completely absent for Pre-LS-4 (Figure S17b, c), further supporting the amphiphilic nature of LS-4. Overall, these detailed computational studies strongly support our hypothesis that such amphiphilic aromatic-azamacrocyclic compounds have the potential of exhibiting increased affinity for the soluble Aβ oligomers, as well as their ability to likely interact *in vivo* with the Aβ aggregates and lipid membranes and thus control their neurotoxicity.

LogD Determination of the ^{64}Cu-LS-4 Complex.

Several studies have reported that Aβ-targeting bifunctional chelators can be utilized as potential ^{64}Cu PET imaging agents for AD.[90–94] With the introduction of the hydrophilic metal-chelating azamacrocycle, the developed amphiphilic compound LS-4 could serve as a bifunctional chelator. Given the promising results from the *ex vivo* studies using the nonradioactive Cu-LS-4 complex, we set out to explore whether the radioactive ^{64}Cu-LS-4 complex could be used as a potential PET imaging agent for AD. First, the radiolabeling of LS-4 was performed using $^{64}CuCl_2$, and the radio-HPLC trace shows that LS-4 can efficiently chelate ^{64}Cu (Figure S18). Since an imaging agent aimed at detecting the Aβ species for AD diagnosis needs to be able to cross the BBB, the lipophilicity of the ^{64}Cu complex was determined by measuring the octanol-PBS partition coefficient logD. The obtained logD value of 1.07 ± 0.13 for the ^{64}Cu-LS-4 complex indicates that the compound is sufficiently hydrophobic to cross the BBB.[73]

Ex Vivo Autoradiography Studies.

Given the promising lipophilicity of the ^{64}Cu-LS-4 complex, *ex vivo* autoradiography studies were performed with 10-month old 5xFAD and WT mouse brain sections to determine if ^{64}Cu-LS-4 can bind to the amyloid species specifically. The 5xFAD mouse brain sections treated with ^{64}Cu-LS-4 showed a significantly stronger autoradiography intensity than the WT mouse brain sections (Figure 12), and the autoradiography intensity was diminished in the presence of a nonradioactive, Aβ-binding blocking agent 2-(4-hydroxyphenyl)benzothiazole,[92] thus confirming a specific binding to the Aβ species. Consequently, the auto-radiography studies suggest that ^{64}Cu-LS-4 can specifically bind to the amyloid plaques, which is also consistent with the *ex vivo* fluorescence brain section staining with the Cu-LS-4 complex, and supporting its ability to detect various Aβ species *in vivo*.

Biodistribution Studies.

Inspired by the promising *in vitro* and *ex vivo* studies, we performed *in vivo* biodistribution experiments to explore the pharmacokinetics of ^{64}Cu-LS-4 by using 5xFAD mice and age-matched WT mice. Notably, the ^{64}Cu-LS-4 complex displayed an appreciable brain uptake of 0.75 ± 0.10%ID/g at 2 min postinjection for the WT mice, which decreased to 0.18 ± 0.02%ID/g at 1 h, thus indicating that ^{64}Cu-LS-4 can cross the BBB and then is washed out rapidly for the brains of WT mice. In AD mice, the ^{64}Cu-LS-4 complex exhibits a brain uptake 0.79 ± 0.06%ID/g at 2 min postinjection, and the brain uptake at 1 and 4 h (0.39 ± 0.02% ID/g) are still detected, which is significantly higher than for the WT mice (Figure 13a). This is most likely due to the binding of the ^{64}Cu-LS-4 complex to the amyloid plaques in the 5xFAD mouse brains. *Ex vivo* autoradiography studies of the brain sections performed at each time point confirm that that the 5xFAD mouse brains exhibit higher autoradiography intensity than WT mouse brains at both 1 and 4 h time points, confirming that ^{64}Cu-LS-4 can penetrate the BBB and label the amyloid species specifically, and thus leading to the delayed washout of ^{64}Cu-LS-4 from the 5xFAD mouse brains (Figure 13b). Overall, these biodistribution studies suggest that ^{64}Cu-LS-4 displays the ability to specifically bind the various Aβ species *in vivo*. However, since the brain uptake of ^{64}Cu-LS-4 is still relatively low, further compound development would be needed to improve the brain uptake for the development of ^{64}Cu PET imaging agents for AD.

CONCLUSION

Herein, we report the development of a novel amphiphilic compound, LS-4, that contains an unsymmetric, hydrophobic distyrylbenzene fragment, which has not been used previously for amyloid-binding studies, and a hydrophilic triazamacrocycle fragment that can interact with the polar residues of the Aβ species. Notably, LS-4 exhibits uncommon fluorescence turn-on and high binding affinity for Aβ aggregates, especially for soluble Aβ oligomers. Moreover, upon the administration of LS-4 to 5xFAD mice, fluorescence imaging of the LS-4-treated brain sections reveals that LS-4 can penetrate the BBB and bind to the Aβ oligomers *in vivo*. The treatment of 5xFAD mice with LS-4 significantly reduces the amount of both amyloid plaques and associated p-tau aggregates vs the vehicle-treated 5xFAD mice, while microglia activation is also reduced. Finally, taking advantage of the strong Cu^{2+}-chelating property of the azamacrocycle, we performed a series of PET imaging and biodistribution studies that show the ^{64}Cu-LS-4 complex binds to the amyloid plaques and can accumulate to a significantly larger extent in the 5xFAD mice brains vs the WT controls. Overall, these *in vitro* and *in vivo* studies provide a detailed molecular understanding and clearly illustrate that the novel strategy to employ an amphiphilic molecule containing a hydrophilic fragment attached to a hydrophobic amyloid fibrilbinding fragment can increase the binding affinity of these compounds for both soluble and insoluble Aβ aggregates, and can thus be used to detect and regulate various Aβ species in AD.

Supplementary Material

Refer to Web version on PubMed Central for supplementary material.

ACKNOWLEDGMENTS

This work was supported by the NIH (R01GM114588 to L.M.M.). E.T. was supported by the National Institutes of Health (P41-GM104601) and also acknowledges computing resources provided by Blue Waters at National Center for Supercomputing Applications. We thank the small animal imaging facilities at Washington University School of Medicine for excellent technical assistance and the Isotope Production Group at Washington University for the production of ^{64}Cu.

REFERENCES

(1). 2020 Alzheimer's disease facts and figures Alzheimer's Dementia 2020, 16, 391–460.

(2). Perrin RJ; Fagan AM; Holtzman DM Multimodal techniques for diagnosis and prognosis of Alzheimer's disease. Nature 2009, 461, 916–922. [PubMed: 19829371]

(3). Selkoe DJ Resolving controversies on the path to Alzheimer's therapeutics. Nat. Med 2011, 17, 1060–1065. [PubMed: 21900936]

(4). Karran E; Mercken M; Strooper BD The Amyloid Cascade Hypothesis for Alzheimer's Disease: An Appraisal for the Development of Therapeutics. Nat. Rev. Drug Discovery 2011, 10, 698–712. [PubMed: 21852788]

(5). Chow VW; Mattson MP; Wong PC; Gleichmann M An Overview of APP Processing Enzymes and Products. NeuroMol. Med 2010, 12, 1–12.

(6). Hardy JA; Higgins GA Alzheimer's Disease: The Amyloid Cascade Hypothesis. Science 1992, 256, 184–185. [PubMed: 1566067]

(7). Bush AI Metals and neuroscience. Curr. Opin. Chem. Biol 2000, 4, 184–191. [PubMed: 10742195]

(8). Ashe KH The biogenesis and biology of amyloid beta oligomers in the brain. Alzheimer's Dementia 2020, 16, 1561–1567.

(9). Zott B; Simon MM; Hong W; Unger F; Chen-Engerer HJ; Frosch MP; Sakmann B; Walsh DM; Konnerth A A vicious cycle of beta amyloid-dependent neuronal hyperactivation. Science 2019, 365, 559–565. [PubMed: 31395777]

(10). Nortley R; Korte N; Izquierdo P; Hirunpattarasilp C; Mishra A; Jaunmuktane Z; Kyrargyri V; Pfeiffer T; Khennouf L; Madry C; Gong H; Richard-Loendt A; Huang W; Saito T; Saido TC; Brandner S; Sethi H; Attwell D Amyloid beta oligomers constrict human capillaries in Alzheimer's disease via signaling to pericytes. Science 2019, 365, eaav9518. [PubMed: 31221773]

(11). Kocis P; Tolar M; Yu J; Sinko W; Ray S; Blennow K; Fillit H; Hey JA Elucidating the Aβ42 Anti-Aggregation Mechanism of Action of Tramiprosate in Alzheimer's Disease: Integrating Molecular Analytical Methods, Pharmacokinetic and Clinical Data. CNS Drugs 2017, 31, 495–509. [PubMed: 28435985]

(12). Tolar M; Abushakra S; Hey JA; Porsteinsson A; Sabbagh M Aducanumab, gantenerumab, BAN2401, and ALZ-801-the first wave of amyloid-targeting drugs for Alzheimer's disease with potential for near term approval. Alzheimer's Res. Ther 2020, 12, 95. [PubMed: 32787971]

(13). Aliyan A; Cook NP; Marti AA Interrogating Amyloid Aggregates using Fluorescent Probes. Chem. Rev 2019, 119, 11819–11856. [PubMed: 31675223]

(14). Xu MM; Ren WM; Tang XC; Hu YH; Zhang HY Advances in development of fluorescent probes for detecting amyloid-beta aggregates. Acta Pharmacol. Sin 2016, 37, 719–730. [PubMed: 26997567]

(15). Yang J; Zeng FT; Ge YR; Peng KW; Li XF; Li YY; Xu YG Development of Near-Infrared Fluorescent Probes for Use in Alzheimers Disease Diagnosis. Bioconjugate Chem. 2020, 31, 2–15.

(16). Cao K; Farahi M; Dakanali M; Chang WM; Sigurdson CJ; Theodorakis EA; Yang J Aminonaphthalene 2-Cyanoacrylate (ANCA) Probes Fluorescently Discriminate between Amyloid-beta and Prion Plaques in Brain. J. Am. Chem. Soc 2012, 134, 17338–17341. [PubMed: 22866977]

(17). Klunk WE; Engler H; Nordberg A; Wang Y; Blomqvist G; Holt DP; Bergström M; Savitcheva I; Huang G-F; Estrada S; Ausén B; Debnath ML; Barletta J; Price JC; Sandell J; Lopresti BJ; Wall A; Koivisto P; Antoni G; Mathis CA; Långström B Imaging Brain Amyloid in Alzheimer's Disease with Pittsburgh Compound-B. Ann. Neurol 2004, 55, 306–319. [PubMed: 14991808]

(18). Rung HF; Choi SR; Qu W; Zhang W; Skovronsky D ^{18}F Stilbenes and Styrylpyridines for PET Imaging of Aβ Plaques in Alzheimer's Disease: A Miniperspective. J. Med. Chem 2010, 53, 933–941. [PubMed: 19845387]

(19). Herholz K; Ebmeier K Clinical amyloid imaging in Alzheimer's disease. Lancet Neurol 2011, 10, 667–670. [PubMed: 21683932]

(20). Teoh CL; Su D; Sahu S; Yun SW; Drummond E; Prelli F; Lim S; Cho S; Ham S; Wisniewski T; Chang YT Chemical Fluorescent Probe for Detection of Abeta Oligomers. J. Am. Chem. Soc 2015, 137, 13503–13509. [PubMed: 26218347]

(21). Li Y; Xu D; Sun A; Ho SL; Poon CY; Chan HN; Ng OTW; Yung KKL; Yan H; Li HW; Wong MS Fluorosubstituted cyanine for reliable in vivo labelling of amyloid-beta oligomers and neuroprotection against amyloid-beta induced toxicity. Chem. Sci 2017, 8, 8279–8284. [PubMed: 29619173]

(22). Lv G; Sun A; Wei P; Zhang N; Lan H; Yi T A spiropyran-based fluorescent probe for the specific detection of beta-amyloid peptide oligomers in Alzheimer's disease. Chem. Commun 2016, 52, 8865–8868.

(23). Li Y; Yang J; Liu H; Yang J; Du L; Feng H; Tian Y; Cao J; Ran C Tuning the stereo-hindrance of a curcumin scaffold for the selective imaging of the soluble forms of amyloid beta species. Chem. Sci 2017, 8, 7710–7717. [PubMed: 29568434]

(24). Yang J; Zeng F; Li X; Ran C; Xu Y; Li Y Highly Specific Detection of Aβ Oligomers in Early Alzheimer's Disease by a Near-Infrared Fluorescent Probe with a "V-shaped" Spatial Conformation. Chem. Commun 2020, 56, 583–586.

(25). Liu HW; Yang J; Wang LT; Xu YG; Zhang SY; Lv J; Ran CZ; Li YY Targeting beta-amyloid plaques and oligomers: development of near-IR fluorescence imaging probes. Future Med. Chem 2017, 9, 179–198. [PubMed: 28127995]

(26). Lee SJC; Nam E; Lee HJ; Savelieff MG; Lim MH Towards an understanding of amyloid-beta oligomers: characterization, toxicity mechanisms, and inhibitors. Chem. Soc. Rev 2017, 46, 310–323. [PubMed: 27878186]

(27). Lv GL; Sun AY; Wang MQ; Wei P; Li RH; Yi T A novel near-infrared fluorescent probe for detection of early-stage Ab protofibrils in Alzheimer's disease. Chem. Commun 2020, 56, 1625–1628.

(28). Han J; Lee HJ; Kim KY; Nam G; Chae J; Lim MH Mechanistic approaches for chemically modifying the coordination sphere of copper-amyloid-beta complexes. Proc. Natl. Acad. Sci. U. S. A 2020, 117, 5160–5167. [PubMed: 32102914]

(29). Sharma AK; Schultz JW; Prior JT; Rath NP; Mirica LM Coordination Chemistry of Bifunctional Chemical Agents Designed for Applications in (64)Cu PET Imaging for Alzheimer's Disease. Inorg. Chem 2017, 56, 13801–13814. [PubMed: 29112419]

(30). Sharma AK; Kim J; Prior JT; Hawco NJ; Rath NP; Kim J; Mirica LM Small Bifunctional Chelators That Do Not Disaggregate Amyloid β Fibrils Exhibit Reduced Cellular Toxicity. Inorg. Chem 2014, 53, 11367–11376. [PubMed: 25333939]

(31). Sharma AK; Pavlova ST; Rim J; Finkelstein D; Hawco NJ; Rath NP; Kim J; Mirica LM Bifunctional Compounds for Controlling Metal-mediated Aggregation of the Aβ_{42} Peptide. J. Am. Chem. Soc 2012, 134, 6625–6636. [PubMed: 22452395]

(32). Beck MW; Oh SB; Kerr RA; Lee HJ; Kim SH; Kim S; Jang M; Ruotolo BT; Lee J-Y; Lim MH A rationally designed small molecule for identifying an in vivo link between metal-amyloid-b complexes and the pathogenesis of Alzheimer's disease. Chem. Sci 2015, 6, 1879–1886. [PubMed: 28706643]

(33). Beck MW; Derrick JS; Kerr RA; Oh SB; Cho WJ; Lee SJC; Ji Y; Han J; Tehrani ZA; Suh N; Kim S; Larsen SD; Kim KS; Lee JY; Ruotolo BT; Lim MH Structure-mechanism-based engineering of chemical regulators targeting distinct pathological factors in Alzheimer's disease. Nat. Commun 2016, 7, 13115. [PubMed: 27734843]

(34). Yang J; Zhang XL; Yuan P; Yang J; Xu YG; Grutzendler J; Shao YH; Moore A; Ran CZ Oxalate-curcumin-based probe for micro- and macroimaging of reactive oxygen species in Alzheimer's disease. Proc. Natl. Acad. Sci. U. S. A 2017, 114, 12384–12389. [PubMed: 29109280]

(35). Yang J; Yang J; Liang SH; Xu YG; Moore A; Ran CZ Imaging hydrogen peroxide in Alzheimer's disease via cascade signal amplification. Sci Rep 2016, 6, 35613. [PubMed: 27762326]

(36). Gomes LMF; Mahammed A; Prosser KE; Smith JR; Silverman MA; Walsby CJ; Gross Z; Storr T A catalytic antioxidant for limiting amyloid-beta peptide aggregation and reactive oxygen species generation. Chem. Sci 2019, 10, 1634–1643. [PubMed: 30842826]

(37). Li L; Xu S; Liu L; Feng R; Gong Y; Zhao X; Li J; Cai J; Feng N; Wang L; Wang X; Peng Y Multifunctional Compound AD-35 Improves Cognitive Impairment and Attenuates the Production of TNF-alpha and IL-1beta in an Abeta25–35-induced Rat Model of Alzheimer's Disease. J. Alzheimer's Dis 2017, 56, 1403–1417. [PubMed: 28157092]

(38). Moussa C; Hebron M; Huang X; Ahn J; Rissman RA; Aisen PS; Turner RS Resveratrol regulates neuro-inflammation and induces adaptive immunity in Alzheimer's disease. J. Neuroinflammation 2017, 14, 1. [PubMed: 28086917]

(39). Camps P; Formosa X; Galdeano C; Gomez T; Munoz-Torrero D; Scarpellini M; Viayna E; Badia A; Clos MV; Camins A; Pallas M; Bartolini M; Mancini F; Andrisano V; Estelrich J; Lizondo M; Bidon-Chanal A; Luque FJ Novel donepezil-based inhibitors of acetyl- and butyrylcholinesterase and acetylcholinesterase-induced beta-amyloid aggregation. J. Med. Chem 2008, 51, 3588–3598. [PubMed: 18517184]

(40). Piazzi L; Rampa A; Bisi A; Gobbi S; Belluti F; Cavalli A; Bartolini M; Andrisano V; Valenti P; Recanatini M 3-(4-{[benzyl(methyl)amino]methyl}-phenyl)-6,7-dimethoxy-2H-2-chromenone (AP2238) inhibits both acetylcholinesterase and acetylcholinesterase-induced beta-amyloid aggregation: A dual function lead for Alzheimer's disease therapy. J. Med. Chem 2003, 46, 2279–2282. [PubMed: 12773032]

(41). Savelieff MG; Nam G; Kang J; Lee HJ; Lee M; Lim MH Development of Multifunctional Molecules as Potential Therapeutic Candidates for Alzheimer's Disease, Parkinson's Disease, and Amyotrophic Lateral Sclerosis in the Last Decade. Chem. Rev 2019, 119, 1221–1322. [PubMed: 30095897]

(42). Jones MR; Mathieu E; Dyrager C; Faissner S; Vaillancourt Z; Korshavn KJ; Lim MH; Ramamoorthy A; Wee Yong V; Tsutsui S; Stys PK; Storr T Multi-target-directed phenol-triazole ligands as therapeutic agents for Alzheimer's disease. Chem. Sci 2017, 8, 5636–5643. [PubMed: 28989601]

(43). Kim M; Kang J; Lee M; Han J; Nam G; Tak E; Kim MS; Lee HJ; Nam E; Park J; Oh SJ; Lee JY; Lee JY; Baik MH; Lim MH Minimalistic Principles for Designing Small Molecules with Multiple Reactivities against Pathological Factors in Dementia. J. Am. Chem. Soc 2020, 142, 8183–8193. [PubMed: 32233474]

(44). Huang YR; Cho HJ; Bandara N; Sun L; Tran D; Rogers BE; Mirica LM Metal-chelating benzothiazole multifunctional compounds for the modulation and Cu-64 PET imaging of A beta aggregation. Chem. Sci 2020, 11, 7789–7799. [PubMed: 34094152]

(45). Cho H-J; Sharma AK; Zhang Y; Gross ML; Mirica LM A Multifunctional Chemical Agent as an Attenuator of Amyloid Burden and Neuroinflammation in Alzheimer's Disease. ACS Chem. Neurosci 2020, 11, 1471–1481. [PubMed: 32310630]

(46). Serra-Batiste M; Ninot-Pedrosa M; Bayoumi M; Gairi M; Maglia G; Carulla N A beta 42 assembles into specific beta-barrel pore-forming oligomers in membrane-mimicking environments. Proc. Natl. Acad. Sci. U. S. A 2016, 113, 10866–10871. [PubMed: 27621459]

(47). Ciudad S; Puig E; Botzanowski T; Meigooni M; Arango AS; Do J; Mayzel M; Bayoumi M; Chaignepain S; Maglia G; Cianferani S; Orekhov V; Tajkhorshid E; Bardiaux B; Carulla N Abeta(1 –42) tetramer and octamer structures reveal edge conductivity pores as a mechanism for membrane damage. Nat. Commun 2020, 11, 3014. [PubMed: 32541820]

(48). Ahmed M; Davis J; Aucoin D; Sato T; Ahuja S; Aimoto S; Elliott JI; Van Nostrand WE; Smith SO Structural conversion of neurotoxic amyloid-beta(1–42) oligomers to fibrils. Nat. Struct. Mol. Biol 2010, 17, 561–7. [PubMed: 20383142]

(49). Arispe N; Rojas E; Pollard HB Alzheimer-Disease Amyloid Beta-Protein Forms Calcium Channels in Bilayer-Membranes - Blockade by Tromethamine and Aluminum. Proc. Natl. Acad. Sci. U. S. A 1993, 90, 567–571. [PubMed: 8380642]

(50). Arispe N; Pollard HB; Rojas E Zn^{2+} interaction with Alzheimer amyloid beta protein calcium channels. Proc. Natl. Acad. Sci. U. S. A 1996, 93, 1710–1715. [PubMed: 8643694]

(51). Hirakura Y; Lin MC; Kagan BL Alzheimer amyloid A beta 1–42 channels: Effects of solvent, pH, and congo red. J. Neurosci. Res 1999, 57, 458–466. [PubMed: 10440895]

(52). Lin H; Bhatia R; Lal R Amyloid beta protein forms ion channels: implications for Alzheimer's disease pathophysiology. FASEB J 2001, 15, 2433–2444. [PubMed: 11689468]

(53). Kourie JI; Henry CL; Farrelly P Diversity of amyloid beta protein fragment [1–40]-formed channels. Cell. Mol. Neurobiol 2001, 21, 255–284. [PubMed: 11569537]

(54). Le Fur M; Beyler M; Le Poul N; Lima LMP; Le Mest Y; Delgado R; Platas-Iglesias C; Patinec V; Tripier R Improving the stability and inertness of Cu(II) and Cu(I) complexes with methylthiazolyl ligands by tuning the macrocyclic structure. Dalton Trans 2016, 45, 7406–7420. [PubMed: 27041505]

(55). Gotzmann C; Braun F; Bartholoma MD Synthesis, Cu-64-labeling and PET imaging of 1,4,7-triazacyclononane derived chelators with pendant azaheterocyclic arms. RSC Adv 2016, 6, 119–131.

(56). Flaherty DP; Kiyota T; Dong YX; Ikezu T; Vennerstrom JL Phenolic Bis-styrylbenzenes as beta-Amyloid Binding Ligands and Free Radical Scavengers. J. Med. Chem 2010, 53, 7992–7999. [PubMed: 21038854]

(57). Boländer A; Kieser D; Scholz C; Heyny-von Haußen R; Mall G; Goetschy V; Czech C; Schmidt B Synthesis of Methoxy-X04 Derivatives and Their Evaluation in Alzheimer's Disease Pathology. Neurodegener. Dis 2014, 13, 209–213. [PubMed: 24080522]

(58). Necula M; Kayed R; Milton S; Glabe CG Small molecule inhibitors of aggregation indicate that amyloid β oligomerization and fibrillization pathways are independent and distinct. J. Biol. Chem 2007, 282, 10311–10324. [PubMed: 17284452]

(59). Miller EW; Lin JY; Frady EP; Steinbach PA; Kristan WB; Tsien RY Optically monitoring voltage in neurons by photo-induced electron transfer through molecular wires. Proc. Natl. Acad. Sci. U. S. A 2012, 109, 2114–2119. [PubMed: 22308458]

(60). Li HJ; Wang L Triethanolamine as an efficient and reusable base, ligand and reaction medium for phosphane-free palladium-catalyzed Heck reactions. Eur. J. Org. Chem 2006, 2006, 5099–5102.

(61). Klein WL; Krafft GA; Finch CE Targeting small A beta oligomers: the solution to an Alzheimer's disease conundrum? Trends Neurosci 2001, 24, 219–224. [PubMed: 11250006]

(62). Oakley H; Cole SL; Logan S; Maus E; Shao P; Craft J; Guillozet-Bongaarts A; Ohno M; Disterhoft J; Van Eldik L; Berry R; Vassar R Intraneuronal β-amyloid aggregates, neurodegeneration, and neuron loss in transgenic mice with five familial Alzheimer's disease mutations: potential factors in amyloid plaque formation. J. Neurosci 2006, 26, 10129–10140. [PubMed: 17021169]

(63). Wilcock DM; Gordon MN; Morgan D Quantification of cerebral amyloid angiopathy and parenchymal amyloid plaques with Congo red histochemical stain. Nat. Protoc 2006, 1, 1591–1595. [PubMed: 17406451]

(64). Schwetye KE; Cirrito JR; Esparza TJ; Mac Donald CL; Holtzman DM; Brody DL Traumatic Brain Injury Reduces Soluble Extracellular Amyloid-β in Mice: A Methodologically Novel Combined Microdialysis-Controlled Cortical Impact Study. Neurobiol. Dis 2010, 40, 555–564. [PubMed: 20682338]

(65). Lindhagen-Persson M; Brannstrom K; Vestling M; Steinitz M; Olofsson A Amyloid-beta oligomer specificity mediated by the IgM isotype–implications for a specific protective mechanism exerted by endogenous auto-antibodies. PLoS One 2010, 5, e13928. [PubMed: 21085663]

(66). Maity D; Howarth M; Vogel MC; Magzoub M; Hamilton AD Peptidomimetic-Based Vesicles Inhibit Amyloid-β Fibrillation and Attenuate Cytotoxicity. J. Am. Chem. Soc 2021, 143, 3086–3093. [PubMed: 33600171]

(67). Re R; Pellegrini N; Proteggente A; Pannala A; Yang M; Rice-Evans C Antioxidant activity applying an improved ABTS radical cation decolorization assay. Free Radical Biol. Med 1999, 26, 1231–1237. [PubMed: 10381194]

(68). Huang DJ; Ou BX; Prior RL The chemistry behind antioxidant capacity assays. J. Agric. Food Chem 2005, 53, 1841–1856. [PubMed: 15769103]

(69). Saharan S; Mandal PK The emerging role of glutathione in Alzheimer's disease. J. Alzheimer's Dis 2014, 40, 519–29. [PubMed: 24496077]

(70). Conte-Daban A; Beyler M; Tripier R; Hureau C Kinetics Are Crucial When Targeting Copper Ions to Fight Alzheimer's Disease: An Illustration with Azamacrocyclic Ligands. Chem. - Eur. J 2018, 24, 8447–8452. [PubMed: 29611877]

(71). Sharma AK; Pavlova ST; Kim J; Kim J; Mirica LM The effect of Cu^{2+} and Zn**2+** on the Aβ_{42} peptide aggregation and cellular toxicity. Metallomics 2013, 5, 1529–1536. [PubMed: 23995980]

(72). Dahlgren KN; Manelli AM; Stine WB; Baker LK; Krafft GA; LaDu MJ Oligomeric and fibrillar species of amyloid-beta peptides differentially affect neuronal viability. J. Biol. Chem 2002, 277, 32046–32053. [PubMed: 12058030]

(73). Dischino DD; Welch MJ; Kilbourn MR; Raichle ME Relationship between Lipophilicity and Brain Extraction of C-11-Labeled Radiopharmaceuticals. J. Nucl. Med 1983, 24, 1030–1038. [PubMed: 6605416]

(74). Ohno M; Chang L; Tseng W; Oakley H; Citron M; Klein WL; Vassar R; Disterhoft JF Temporal memory deficits in Alzheimer's mouse models: rescue by genetic deletion of BACE1. Eur. J. Neurosci 2006, 23, 251–260. [PubMed: 16420434]

(75). Makin S The amyloid hypothesis on trial. Nature 2018, 559, S4–S4. [PubMed: 30046080]

(76). Morris GP; Clark IA; Vissel B Inconsistencies and Controversies Surrounding the Amyloid Hypothesis of Alzheimer's Disease. Acta Neuropathol. Commun 2014, 2, 135. [PubMed: 25231068]

(77). He Z; Guo JL; McBride JD; Narasimhan S; Kim H; Changolkar L; Zhang B; Gathagan RJ; Yue C; Dengler C; Stieber A; Nitla M; Coulter DA; Abel T; Brunden KR; Trojanowski JQ; Lee VMY Amyloid-β plaques enhance Alzheimer's brain tau-seeded pathologies by facilitating neuritic plaque tau aggregation. Nat. Med 2018, 24, 29. [PubMed: 29200205]

(78). Leyns CEG; Gratuze M; Narasimhan S; Jain N; Koscal LJ; Jiang H; Manis M; Colonna M; Lee VMY; Ulrich JD; Holtzman DM TREM2 function impedes tau seeding in neuritic plaques. Nat. Neurosci 2019, 22, 1217–1222. [PubMed: 31235932]

(79). Shukla V; Zheng Y-L; Mishra SK; Amin ND; Steiner J; Grant P; Kesavapany S; Pant HC A truncated peptide from p35, a Cdk5 activator, prevents Alzheimer's disease phenotypes in model mice. FASEB J 2013, 27, 174–186. [PubMed: 23038754]

(80). Giacobini E; Gold G Alzheimer disease therapy—moving from amyloid-β to tau. Nat. Rev. Neurol 2013, 9, 677–686. [PubMed: 24217510]

(81). Ostrowitzki S; Deptula D; Thurfjell L; Barkhof F; Bohrmann B; Brooks DJ; Klunk WE; Ashford E; Yoo K; Xu Z-X; Loetscher H; Santarelli L Mechanism of amyloid removal in patients with Alzheimer disease treated with Gantenerumab. Arch. Neurol 2012, 69, 198–207. [PubMed: 21987394]

(82). Doody RS; Thomas RG; Farlow M; Iwatsubo T; Vellas B; Joffe S; Kieburtz K; Raman R; Sun X; Aisen PS; Siemers E; Liu-Seifert H; Mohs R Phase 3 trials of Solanezumab for mild-to-moderate Alzheimer's disease. N. Engl. J. Med 2014, 370, 311–321. [PubMed: 24450890]

(83). Salloway S; Sperling R; Fox NC; Blennow K; Klunk W; Raskind M; Sabbagh M; Honig LS; Porsteinsson AP; Ferris S; Reichert M; Ketter N; Nejadnik B; Guenzler V; Miloslavsky M; Wang D; Lu Y; Lull J; Tudor IC; Liu E; Grundman M; Yuen E; Black R; Brashear HR Two phase 3 trials of Bapineuzumab in mild-to-moderate Alzheimer's disease. N. Engl. J. Med 2014, 370, 322–333. [PubMed: 24450891]

(84). Dhawan G; Floden AM; Combs CK Amyloid-beta oligomers stimulate microglia through a tyrosine kinase dependent mechanism. Neurobiol. Aging 2012, 33, 2247–2261. [PubMed: 22133278]

(85). Doens D; Fernandez PL Microglia receptors and their implications in the response to amyloid beta for Alzheimer's disease pathogenesis. J. Neuroinflammation 2014, 11, 48. [PubMed: 24625061]

(86). Leyns CEG; Ulrich JD; Finn MB; Stewart FR; Koscal LJ; Remolina Serrano J; Robinson GO; Anderson E; Colonna M; Holtzman DM TREM2 deficiency attenuates neuroinflammation and protects against neurodegeneration in a mouse model of tauopathy. Proc. Natl. Acad. Sci. U. S. A 2017, 114, 11524–11529. [PubMed: 29073081]

(87). Phillips JC; Braun R; Wang W; Gumbart J; Tajkhorshid E; Villa E; Chipot C; Skeel RD; Kale L; Schulten K Scalable molecular dynamics with NAMD. J. Comput. Chem 2005, 26, 1781–1802. [PubMed: 16222654]

(88). Phillips JC; Hardy DJ; Maia JDC; Stone JE; Ribeiro JV; Bernardi RC; Buch R; Fiorin G; Henin J; Jiang W; McGreevy R; Melo MCR; Radak BK; Skeel RD; Singharoy A; Wang Y; Roux B; Aksimentiev A; Luthey-Schulten Z; Kale LV; Schulten K; Chipot C; Tajkhorshid E Scalable molecular dynamics on CPU and GPU architectures with NAMD. J. Chem. Phys 2020, 153, 044130. [PubMed: 32752662]

(89). Paravastu AK; Leapman RD; Yau WM; Tycko R Molecular structural basis for polymorphism in Alzheimer's beta-amyloid fibrils. Proc. Natl. Acad. Sci. U. S. A 2008, 105, 18349–18354. [PubMed: 19015532]

(90). Hickey JL; Lim S; Hayne DJ; Paterson BM; White JM; Villemagne VL; Roselt P; Binns D; Cullinane C; Jeffery CM; Price RI; Barnham KJ; Donnelly PS Diagnostic Imaging Agents for Alzheimer's Disease: Copper Radiopharmaceuticals that Target Aβ Plaques. J. Am. Chem. Soc 2013, 135, 16120–16132. [PubMed: 24070589]

(91). McInnes LE; Noor A; Kysenius K; Cullinane C; Roselt P; McLean CA; Chiu FCK; Powell AK; Crouch PJ; White JM; Donnelly PS Potential Diagnostic Imaging of Alzheimer's Disease with Copper-64 Complexes That Bind to Amyloid-beta Plaques. Inorg. Chem 2019, 58, 3382–3395. [PubMed: 30785268]

(92). Bandara N; Sharma AK; Krieger S; Schultz JW; Han BH; Rogers BE; Mirica LM Evaluation of ^{64}Cu-based Radiopharmaceuticals That Target Aβ Peptide Aggregates as Diagnostic Tools for Alzheimer's Disease. J. Am. Chem. Soc 2017, 139, 12550–12558. [PubMed: 28823165]

(93). Noor A; Hayne DJ; Lim S; Van Zuylekom JK; Cullinane C; Roselt PD; McLean CA; White JM; Donnelly PS Copper Bis(thiosemicarbazonato)-stilbenyl Complexes That Bind to Amyloid-beta Plaques. Inorg. Chem 2020, 59, 11658–11669. [PubMed: 32799487]

(94). Cho HJ; Huynh TT; Rogers BE; Mirica LM Design of a multivalent bifunctional chelator for diagnostic (64)Cu PET imaging in Alzheimer's disease. Proc. Natl. Acad. Sci. U. S. A 2020, 117, 30928–30933. [PubMed: 33234563]

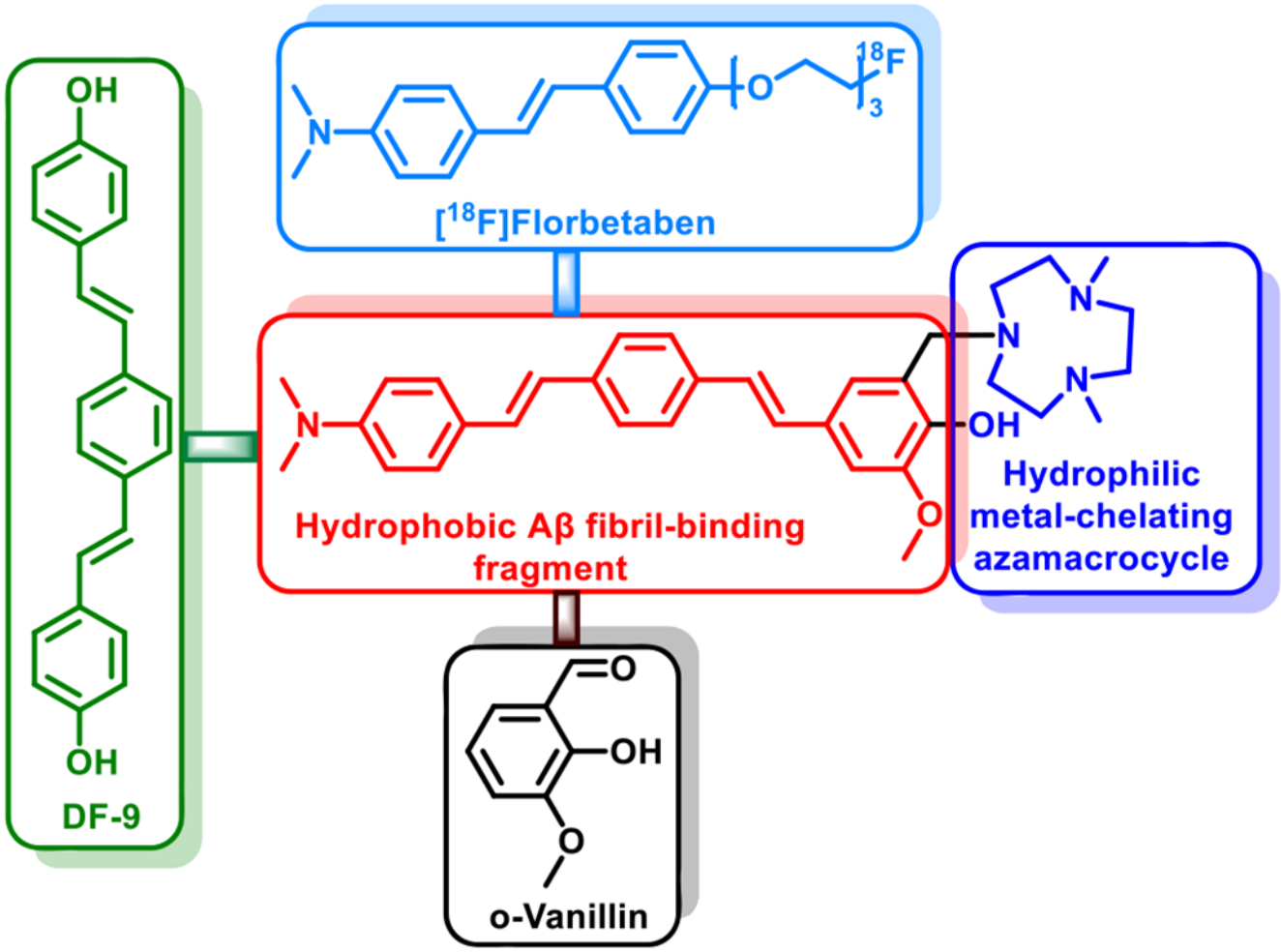

Figure 1.

Design strategy and structure of the amphiphilic compound LS-4. The Aβ fibril-interacting hydrophobic region of LS-4 is shown in red and the hydrophilic metal-chelating azamacrocycle is shown in blue. The Aβ binding framework contains fragments resembling the PET imaging agent [^{18}F]florbetaben (light blue) approved by the U.S. Food and Drug Administration, the widely used amyloid dye DF-9 (green), as well as the 2-methoxy-phenol fragment reminiscent of ovanillin that can inhibit the formation of Aβ oligomers and also exhibits antioxidant properties (black).

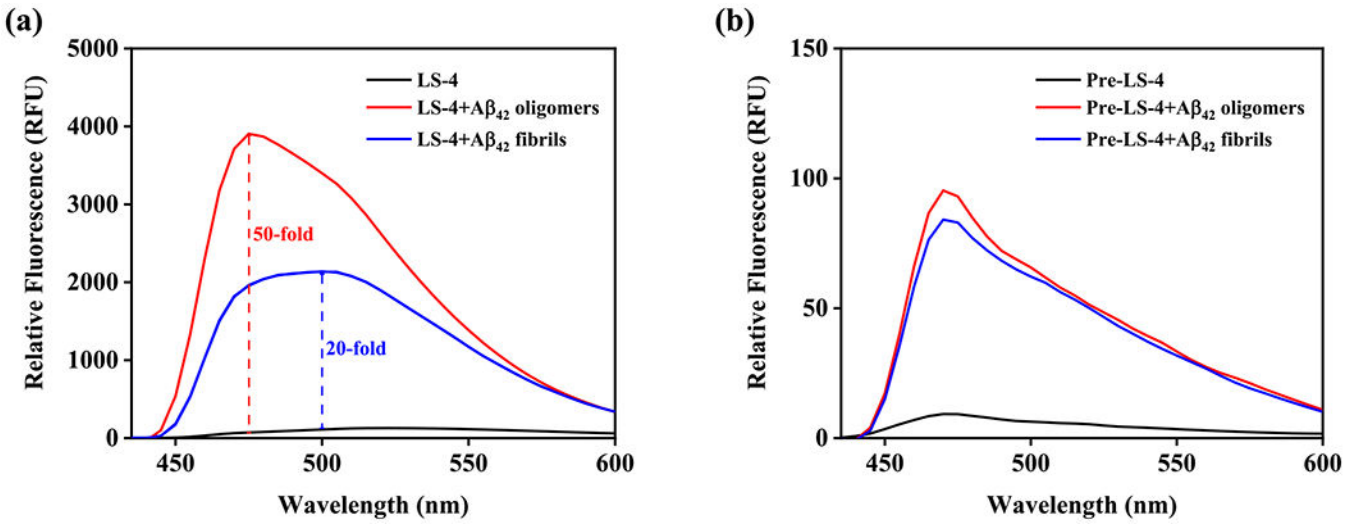

Figure 2.

Fluorescence turn-on effects of LS-4 and Pre-LS-4 with Aβ_{42} oligomers and fibrils. (a) LS-4 (black), Aβ_{42} oligomers + LS-4 (red) and Aβ_{42} fibrils + LS-4 (blue); (b) Pre-LS-4 (black), Aβ_{42} oligomers + Pre-LS-4 (red) and Aβ_{42} fibrils + Pre-LS-4 (blue). [Aβ_{42}] = 25 μM, [LS-4] = [Pre-LS-4] = 5 μM, excitation wavelength = 380 nm in pH = 7.4 PBS buffer.

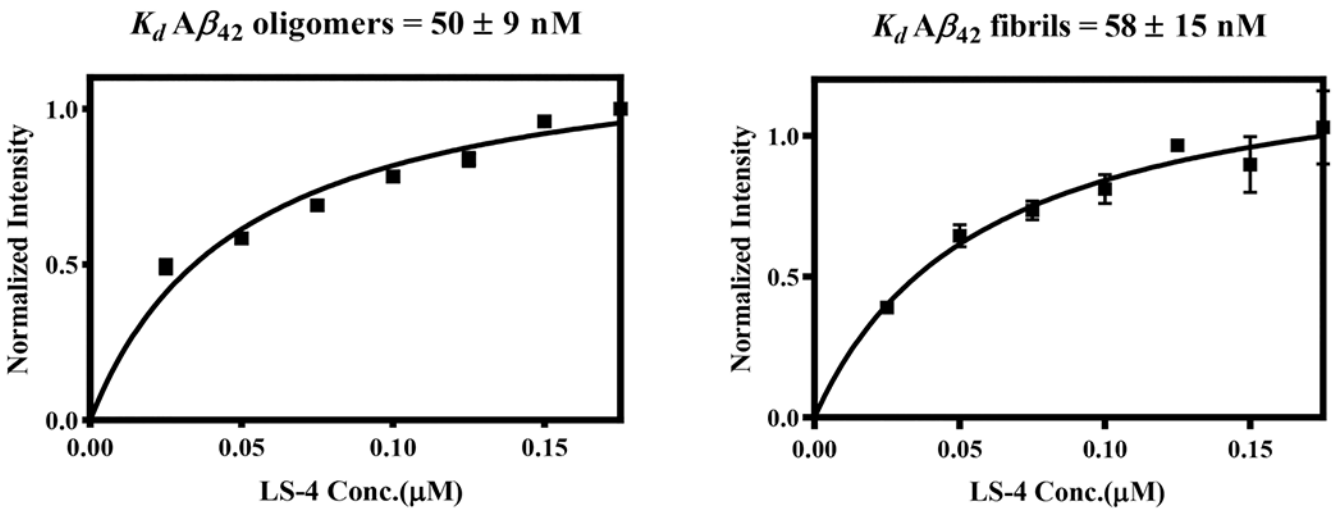

Figure 3.

Direct binding K_d measurements for LS-4 with Aβ_{42} oligomers (left) and fibrils (right). Each experiment was completed in duplicates, and the error bars represent the standard deviation (n = 3) for the average normalized fluorescence intensities. All data points include error bars, and some of the error bars are smaller than the square symbol.

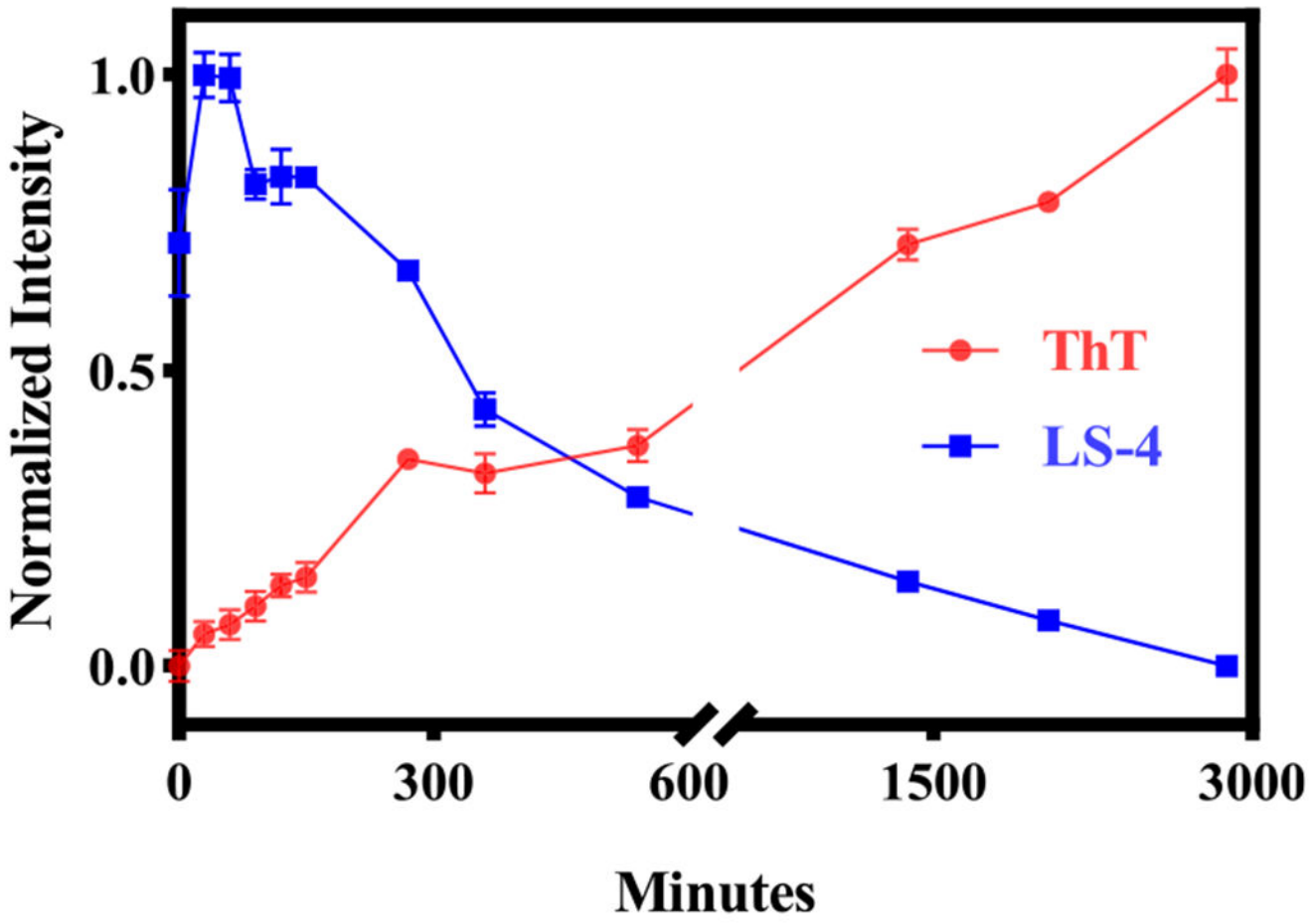

Figure 4.

Monitoring of the aggregation of Aβ_{42} at different time points with LS-4 (blue) and ThT (red). The fluorescence intensities of ThT (λ_{ex} = 435 nm) and LS-4 (λ_{ex} = 380 nm) were recorded at 485 and 470 nm, respectively. Conditions: [Aβ] = 25 μM, [ThT] = [LS-4] = 5 μM. The peptides were incubated in pH = 7.4 PBS buffer at 37 °C with shaking at 1000 rpm for 48 h. The error bars represent the standard deviation (n = 3) for the average normalized fluorescence intensity.

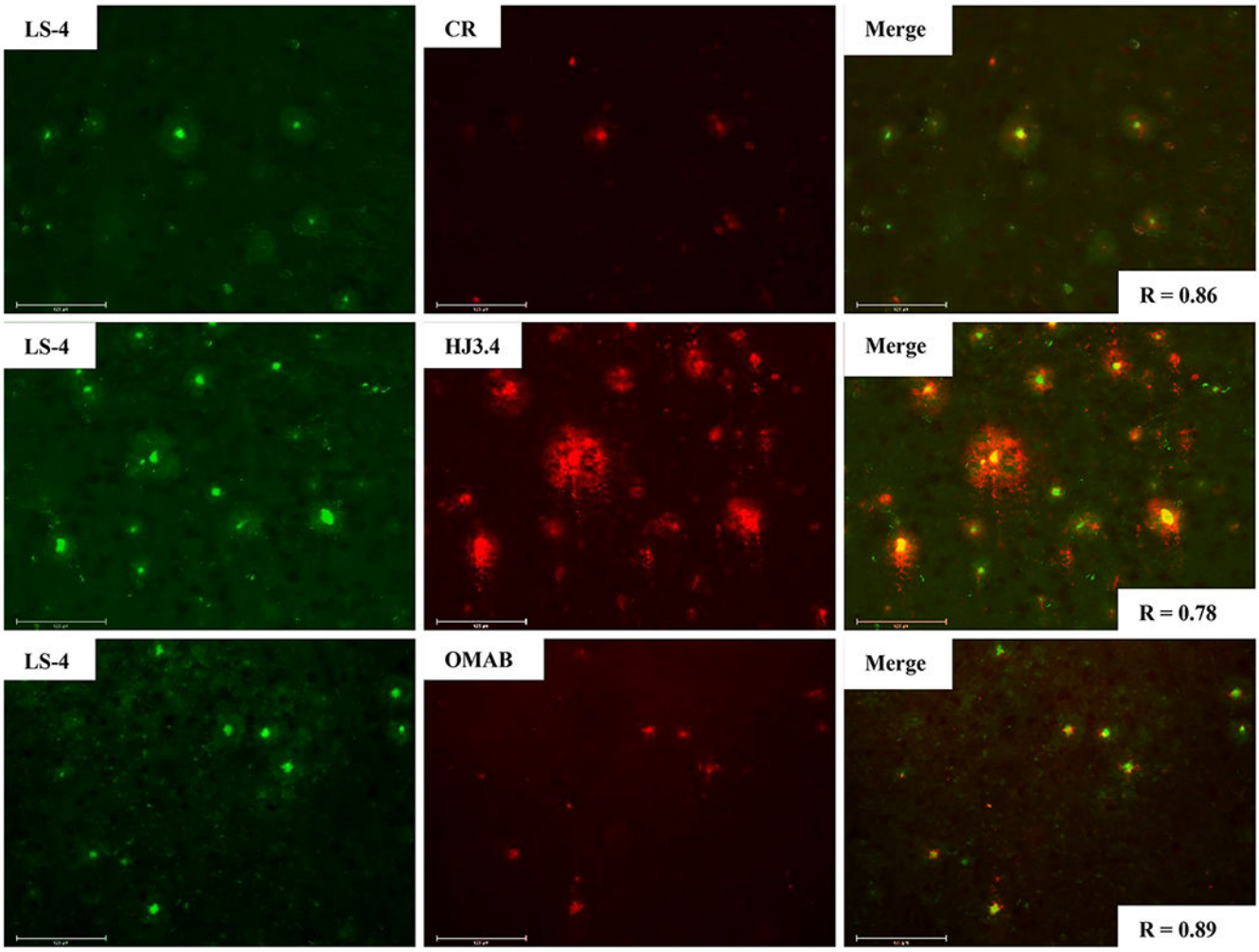

Figure 5.

Fluorescence microscopy images of 5xFAD mouse brain sections incubated with LS-4 (left panels), Congo Red, HJ3.4, or OMAB (middle panels), and merged images (right panels). [LS-4] = 25 μM, [Congo Red] = 5 μM, [HJ3.4] = 1 μ/mL, [OMAB] = 2 μ/mL. LS-4 has significant colocalization with the amyloid species stained with Congo Red, the HJ3.4 antibody, or OMAB. Scale bar: 125 μm.

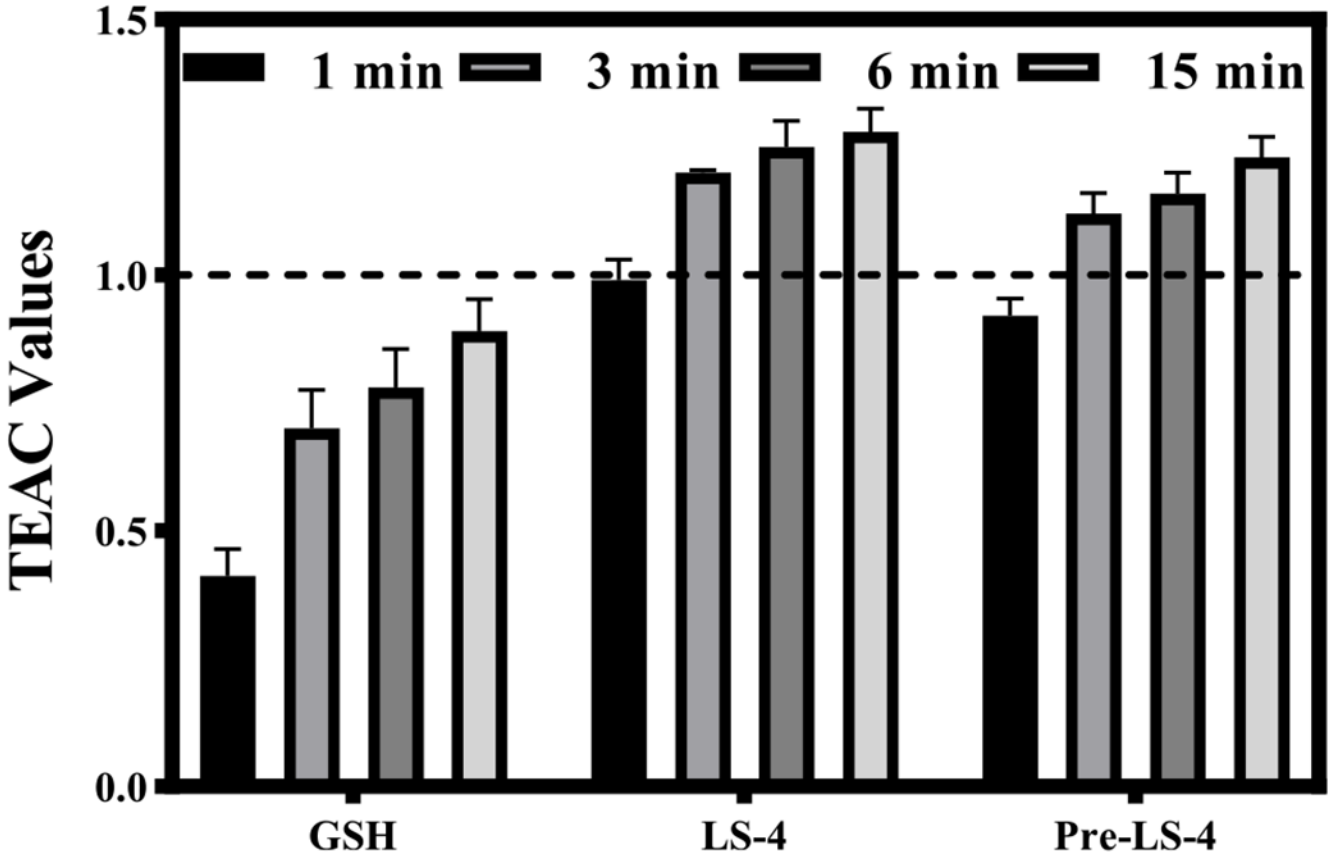

Figure 6.

Trolox-equivalent antioxidant capacity (TEAC) values at 1, 3, 6, and 15 min for glutathione (GSH), LS-4, and Pre-LS-4. The TEAC values of glutathione, LS-4 and Pre-LS-4 are normalized to the antioxidant activity of Trolox (shown by the dashed line). Each experiment was completed in triplicate, and the error bars represent the standard deviation (n = 3) for the average TEAC values.

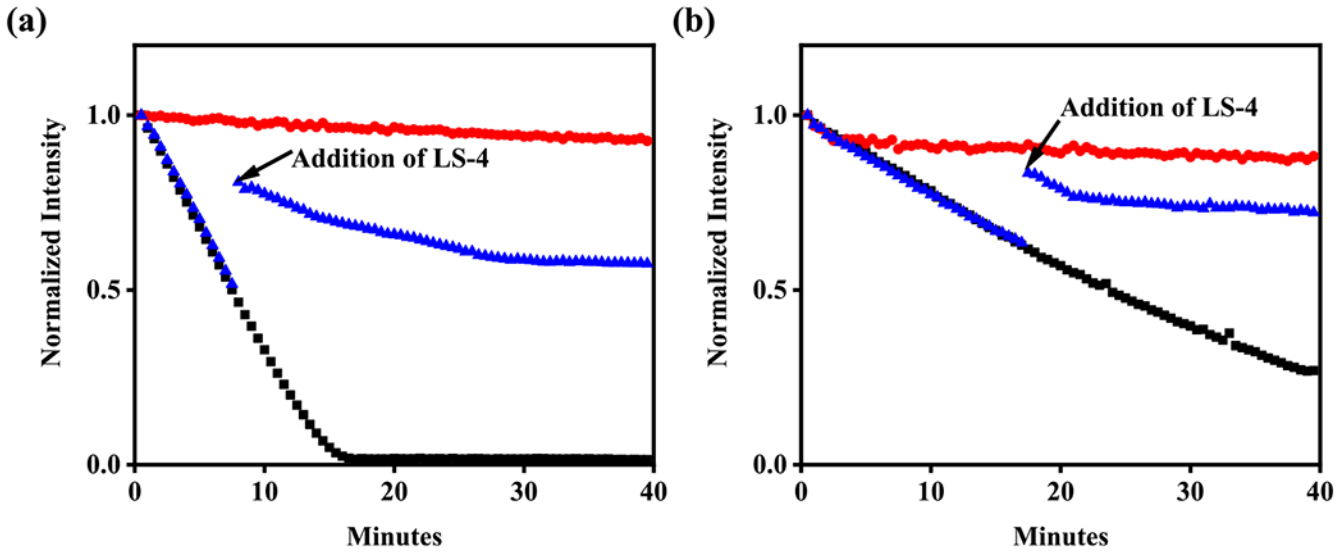

Figure 7.

Kinetics of ascorbate consumption monitored by UV–vis at 265 nm. (a) Cu^{2+} + ascorbate (black), Cu^{2+} + LS-4 + ascorbate (red), Cu^{2+} + ascorbate + LS-4 (blue); (b) Cu^{2+} + Aβ_{42} + ascorbate (black), Cu^{2+} + Aβ_{42} + LS-4 + ascorbate (red), Cu^{2+} + Aβ_{42} + ascorbate + LS-4 (blue). (b) [Cu^{2+}] = 10 μM, [Aβ_{42}] = 12 μM, [LS-4] = 24 μM, [ascorbate] = 100 μM.

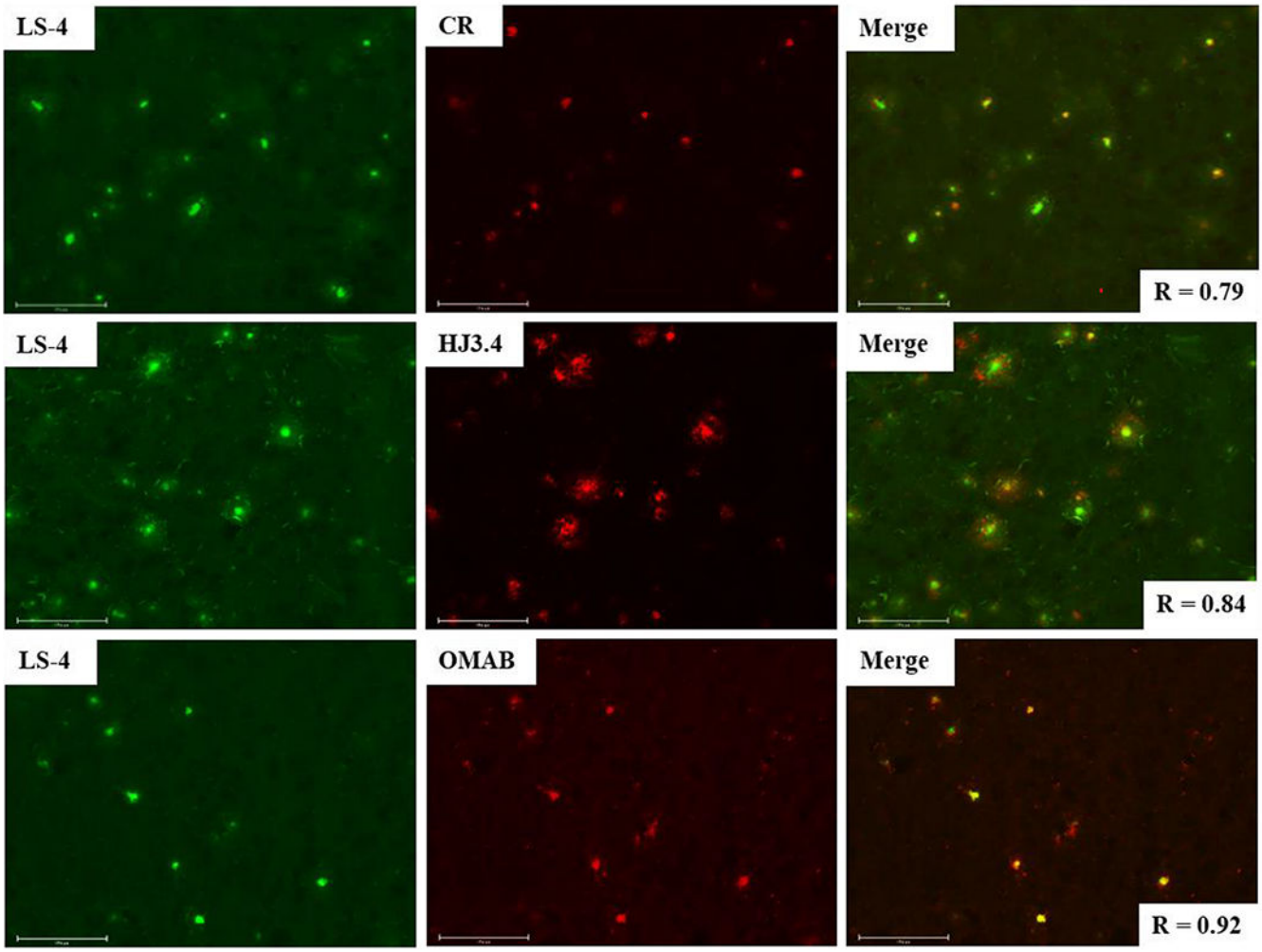

Figure 8.

Representative fluorescence microscopy images of brain sections from 7-month old 5xFAD mice administered with LS-4 for 10 days. The brain sections were immunostained with Congo Red, the HJ3.4 antibody, and the OMAB antibody ([Congo Red] = 5 μM, [HJ3.4] = 1 μg/mL, [OMAB] = 2 μg/mL, scale bar = 125 μm). The *in vivo* accumulated LS-4 has significant colocalization with the amyloid species costained with Congo Red (Pearson's R = 0.79), HJ3.4 (Pearson's R = 0.84), or OMAB (Pearson's R = 0.92).

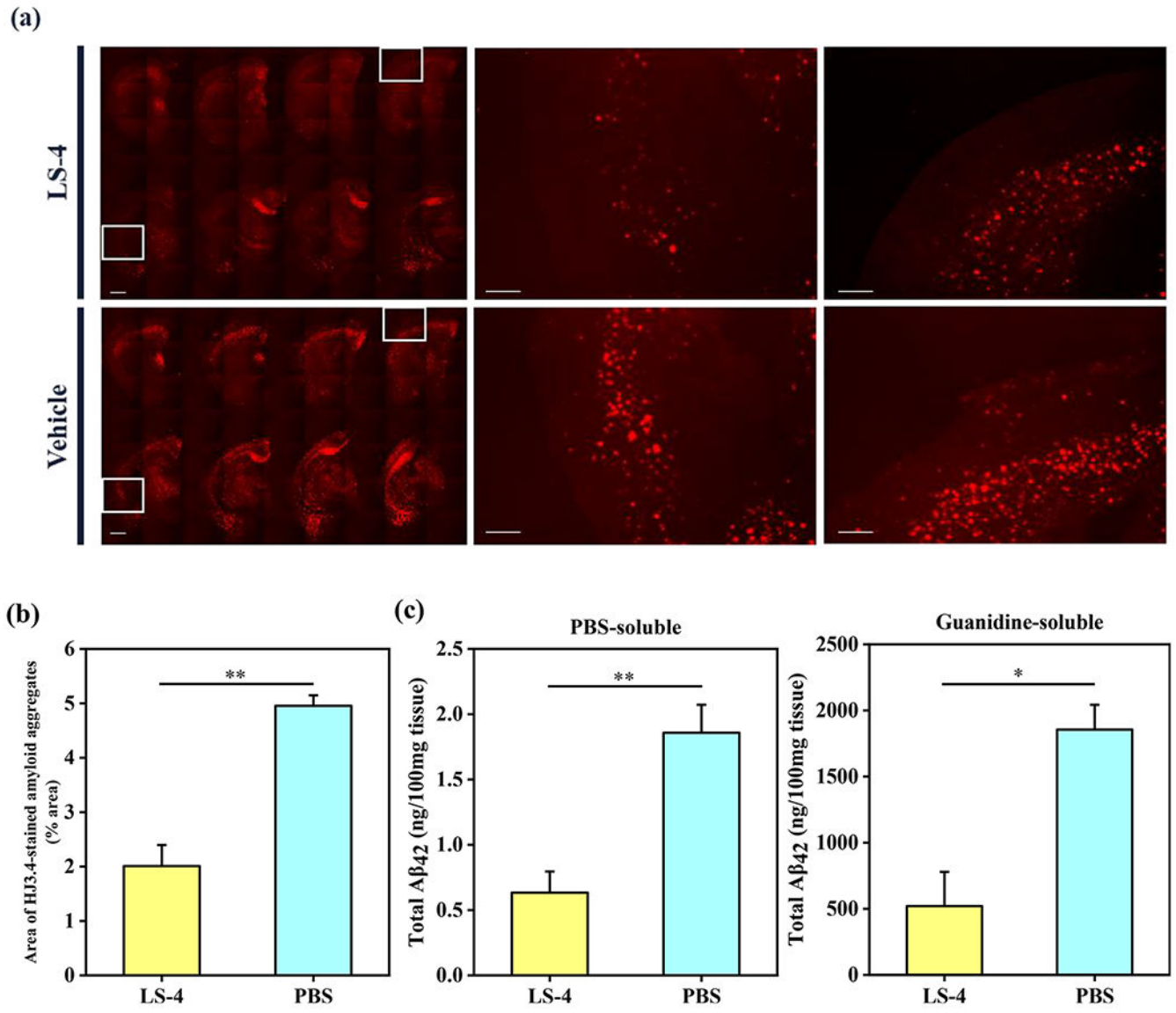

Figure 9.

Reduction of cerebral amyloid pathology by LS-4 in 5xFAD mice. The brain tissues were collected from the 3-month old 5xFAD mice after 30 days i.p. injections of LS-4 or vehicle. (a) Representative fluorescence microscopy images of the CF594-HJ3.4 antibody-stained brain sections from 5xFAD mice treated with LS-4 and vehicle. Scale bar = 500 μm. (b) Total area of HJ3.4-staining amyloid plaques in the brain sections from 5xFAD mouse treated with LS-4 and vehicle. The area of antibody-stained amyloid plaques was selected from 8 brain sections per mice. For each brain section, five random areas across the cortex regions were chosen. Error bars represent the standard deviation (LS-4-treated mice, n = 4, vehicle-treated mice, n = 3), and the statistical analysis was evaluated according to one-way ANOVA (** $p < 0.01$). (c) The bars indicate the amount of PBS-soluble (left) and guanidine-soluble (right) Aβ_{42} peptide levels from brain tissues. Error bars represent

standard deviations (LS-4 treated mice, $n = 5$, vehicle-treated mice, $n = 3$), and the statistical analysis was evaluated according to one-way ANOVA (** $p < 0.01$, * $p < 0.05$).

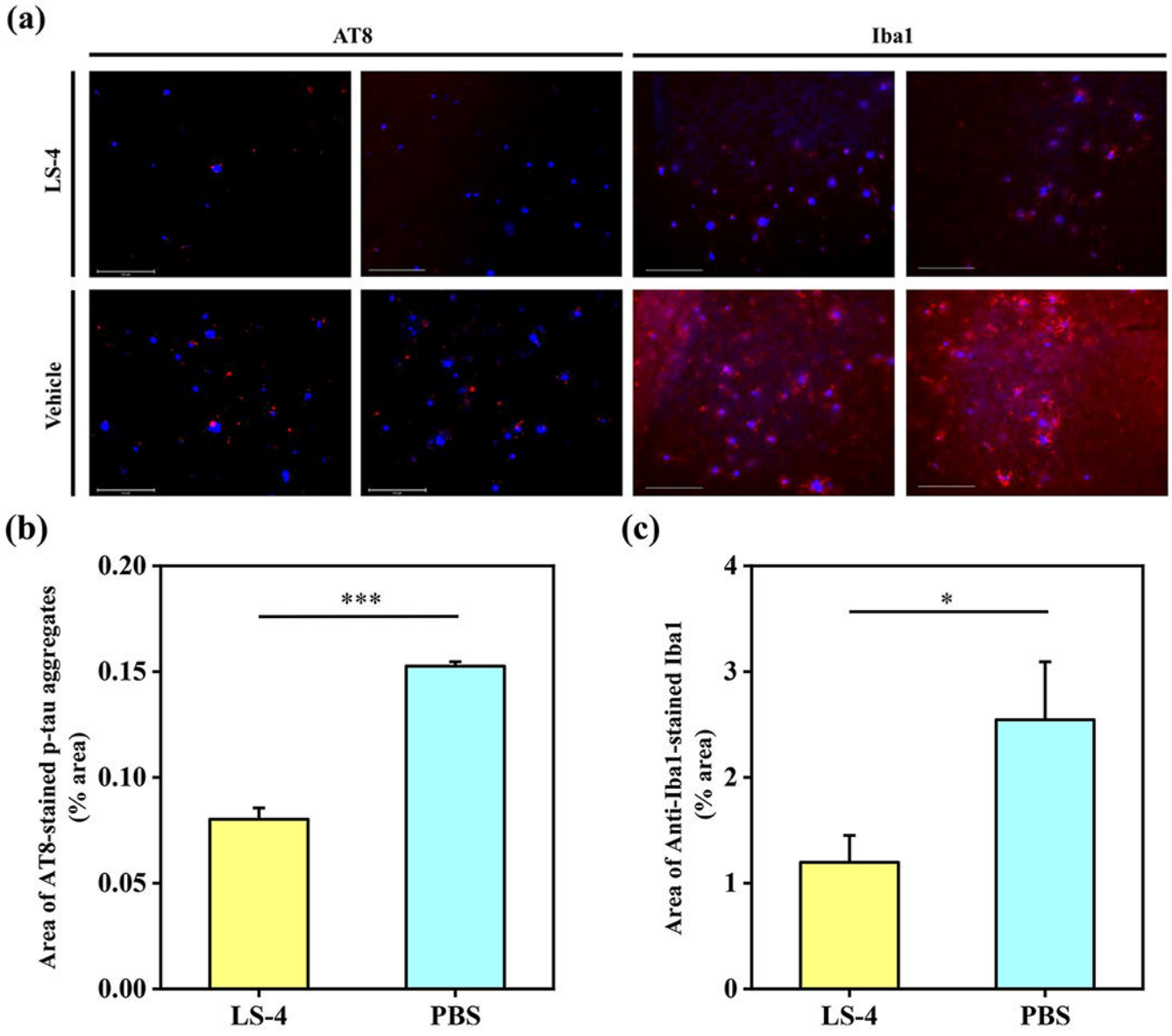

Figure 10.

(a) Representative fluorescence microscopy images of the CF594-AT8 and CF594-Iba1 immunostained brain sections from 5xFAD mice treated with LS-4 and vehicle. All fluorescence images are the maximum intensity projection images obtained from 30 Z-sections collected at 1 μm intervals. Color: red, CF594-Iba1 or CF594-AT8 antibody; blue, ThS. Scale bar: 125 μm. (b) Quantification of the area of CF594-AT8 immunostained brain sections from 5xFAD mice. All data were obtained from 8 brain sections per mice. For each brain section, four random areas across cortex regions were chosen. Error bars represent the standard deviation (LS-4 treated mice, $n = 4$, vehicle-treated mice, $n = 3$), and the statistical analysis was evaluated according to one-way ANOVA (***$p < 0.001$). (c) Quantification of the area of CF594-Iba1 immunostained brain sections from 5xFAD mice. All data were obtained from 8 brain sections per mice. For each brain section, four random areas across cortex region were chosen. Error bars represent the standard deviation (LS-4 treated mice,

$n = 4$, vehicle-treated mice, $n = 3$), and the statistical analysis was evaluated according to one-way ANOVA ($^{*}p < 0.05$).

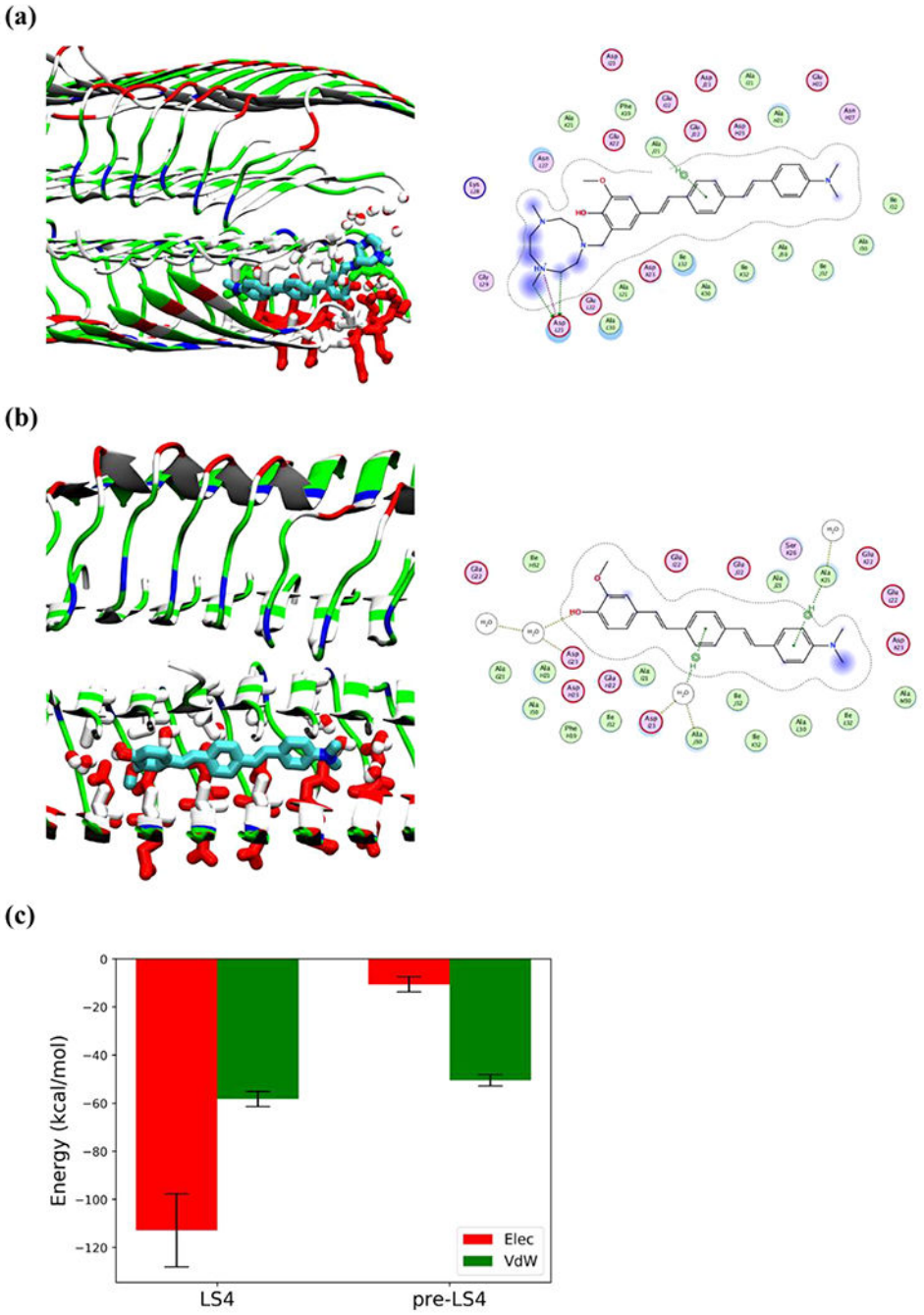

Figure 11.

Detailed interactions of LS-4 and Pre-LS-4 docked onto the Aβ fibril after 100 ns simulations. Compounds are shown by licorice representation colored by atoms (C: cyan, N: blue, O: red), the water molecules and amino acid side chains within 3 Å of the compounds are displayed by licorice representation. Acidic, basic, polar, and nonpolar amino acid residues are shown in red, blue, green, and white colors, respectively, water molecules are colored by atoms (O: red, H: white). For 2D compound-protein interaction patterns, the close-by protein residues and solvent molecules are shown in proximity around the

compound. The compound is annotated with a proximity contour and solvent exposure while the protein residues are also annotated by solvent exposure. The green dotted lines with arrows represent H-bonding with protein side chains, whereas the purple dotted line highlights the presence of a salt bridge. (a) Interaction of LS-4 with the Aβ fibril; (b) Interaction of Pre-LS-4 with the Aβ fibril; (c) Electrostatic and van der Waals interaction energies of LS-4 and Pre-LS-4 with Aβ fibril, averaged over the last 25 ns of the MD simulations.

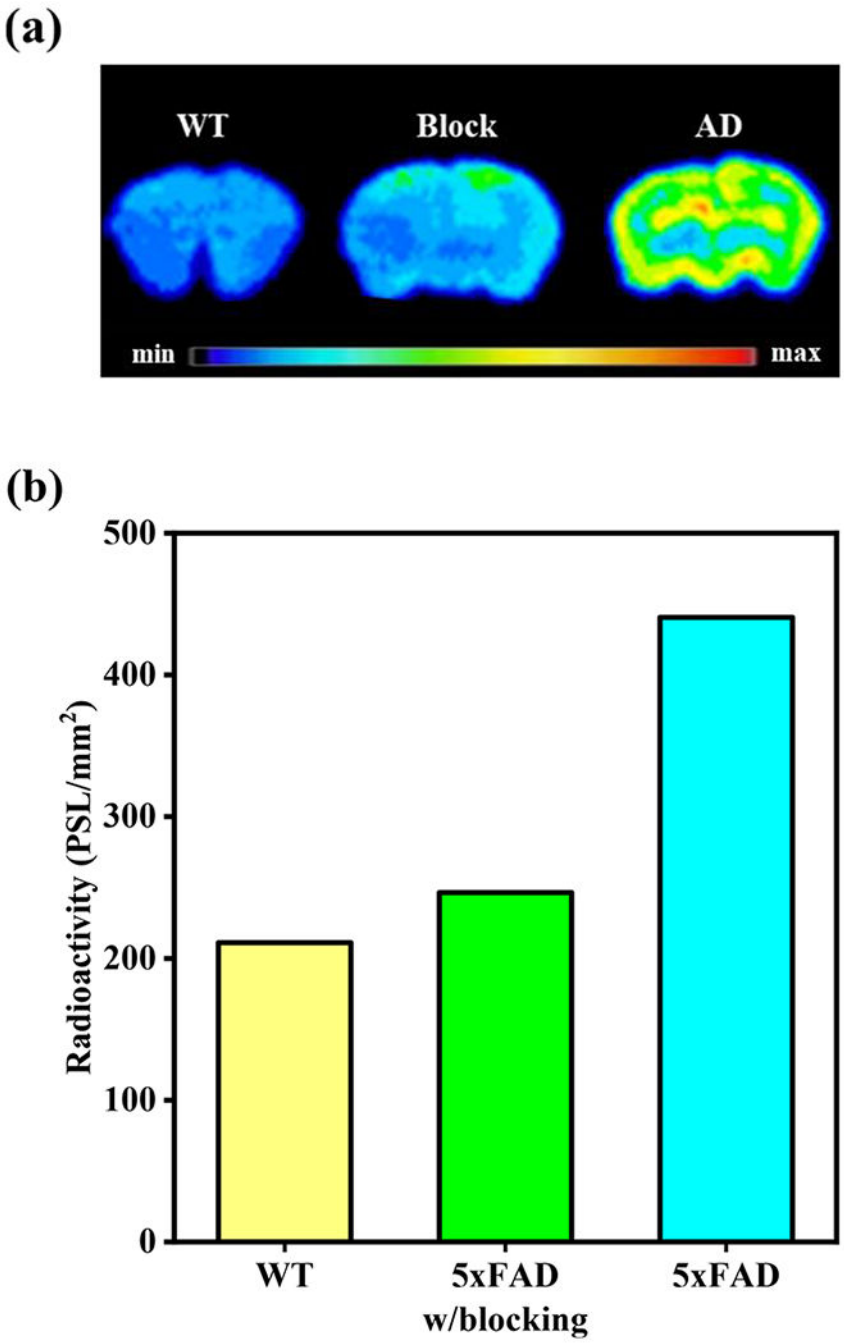

Figure 12.

(a) Autoradiography images of WT and 5xFAD mouse brain sections, in the presence or absence of a nonradioactive Aβ-specific blocking agent 2-(4-hydroxyphenyl)benzothiazole.[92] (b) Quantification of the signal intensity of the autoradiography images for the WT and 5xFAD mouse brain sections, in the presence or absence of a nonradioactive Aβ-specific blocking agent.

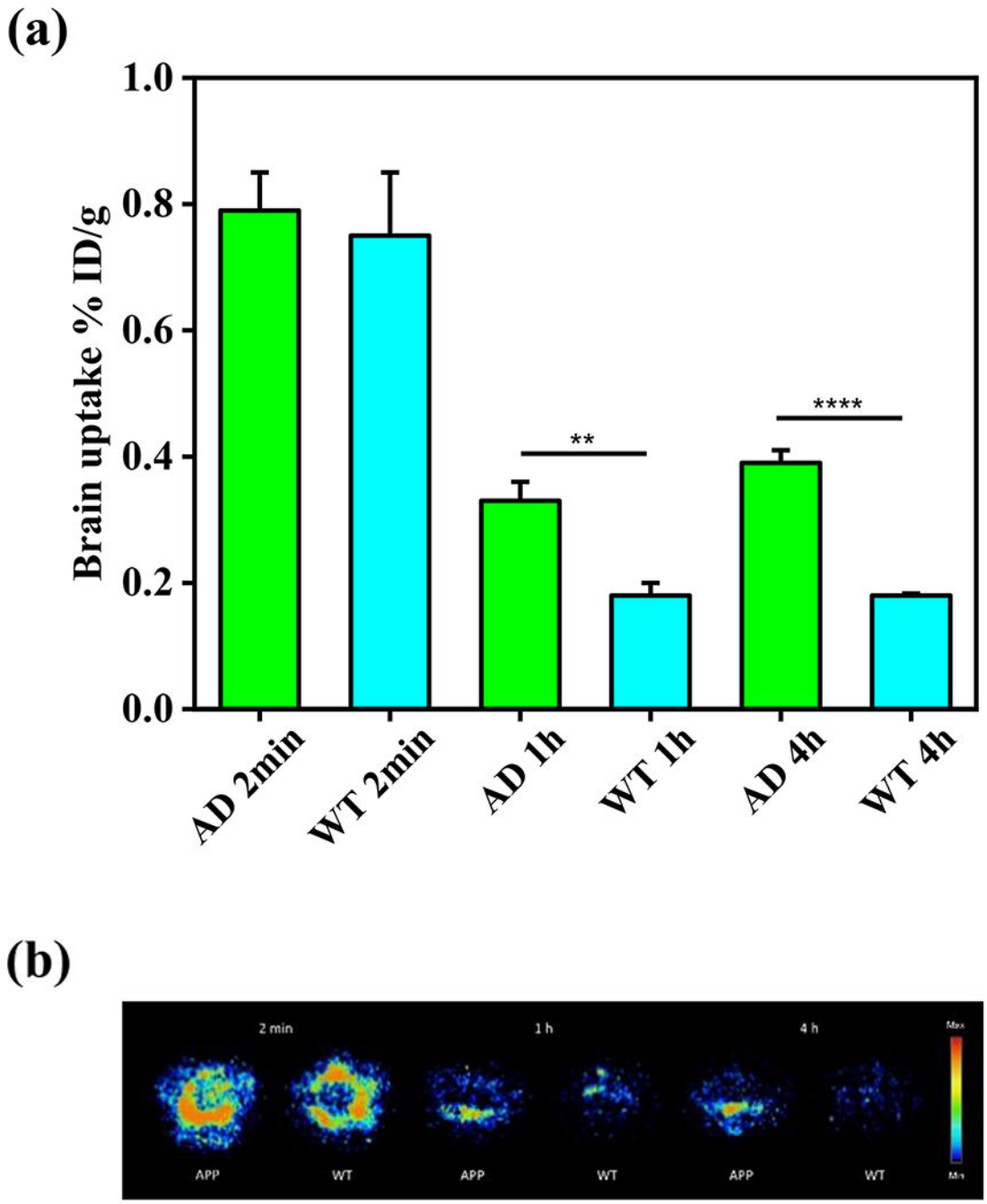

Figure 13.

(a) Brain uptake results (% injected dose per gram, ID/g) from the *in vivo* biodistribution study of ^{64}Cu-LS-4 in 11-month old 5xFAD mice (green) vs age-matched WT mice (cyan), at 2 min, 1 h, and 4 h postinjection. Error bars represent standard deviations ($n = 3$), and the statistical analysis was evaluated according to one-way ANOVA (**$p < 0.01$, ****$p < 0.001$). (b) Autoradiography images of brain sections from 5xFAD and WT mice at different time points during the biodistribution studies.

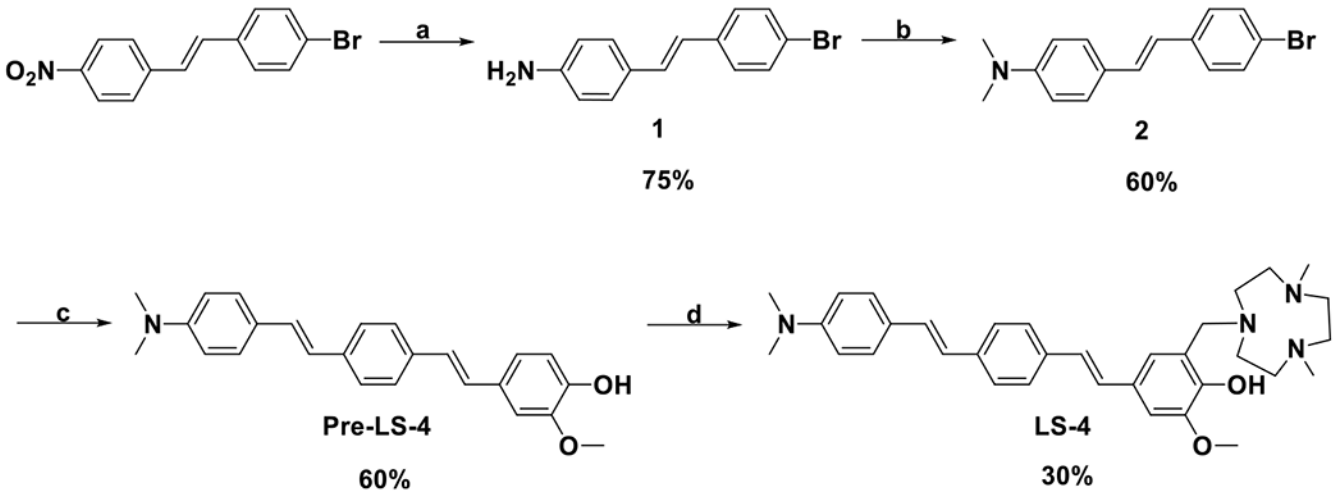

Scheme 1.

Synthesis of Pre-LS-4 and LS-4[a]

[a](a) $SnCl_2$, conc. HCl, EtOH, reflux, 3 h; (b) $(CH_2O)_n$, $NaBH_3CN$, CH_3COOH, room temperature, overnight; (c) 2-methoxy-4-vinylphenol, $Pd(OAc)_2$, triethanolamine, 100 °C, 24 h; (d) Me_2HTACN, $(CH_2O)_n$, MeCN, reflux, 24 h.